NONLINEAR ANALYSIS OF ROTATING MACHINERY RUNNING ON FOIL-AIR BEARING
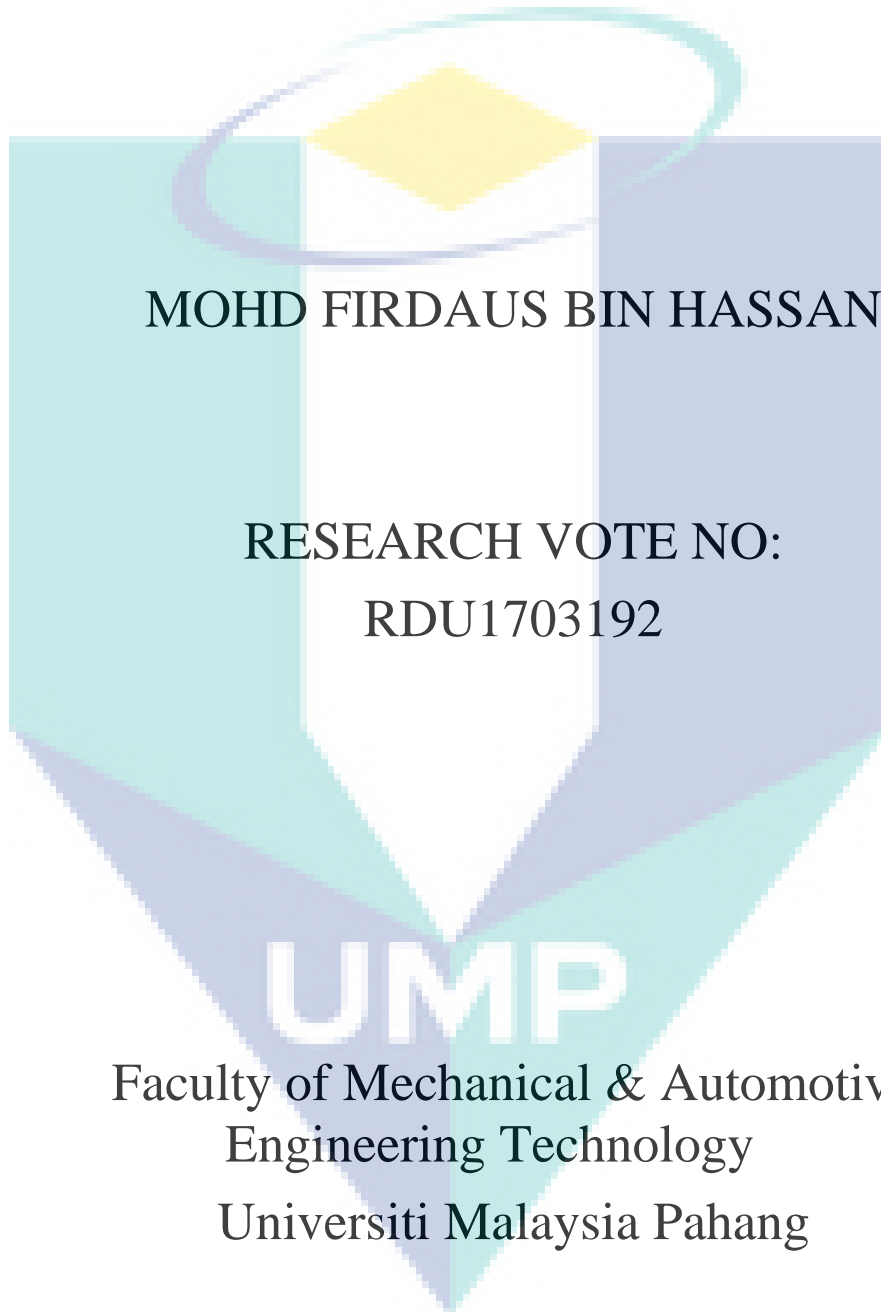
MOHD FIRDAUS BIN HASSAN

RESEARCH VOTE NO:
RDU1703192

Faculty of Mechanical & Automotive
Engineering Technology
Universiti Malaysia Pahang

ACKNOWLEDGEMENTS
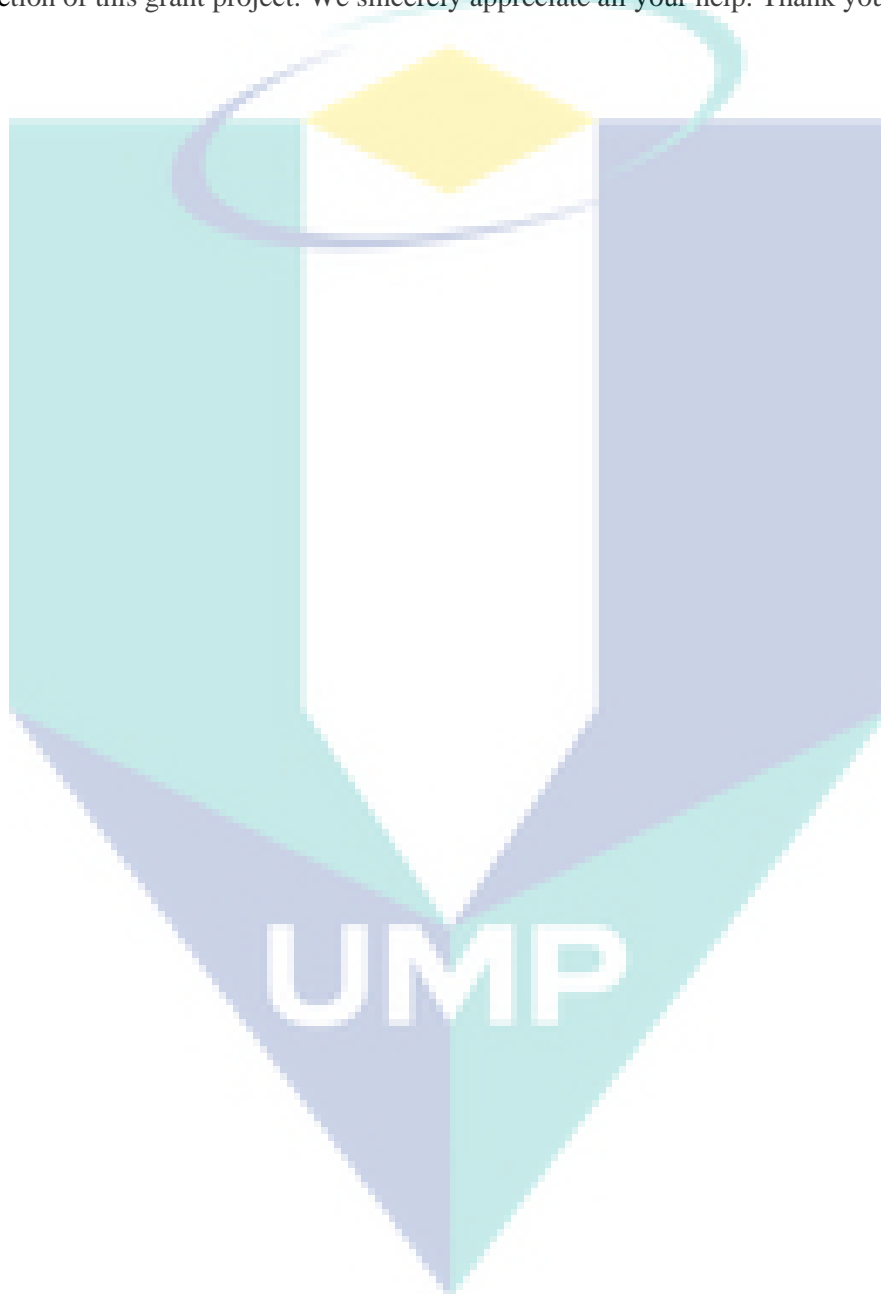
ABSTRAK

Kajian ini adalah mengenai kesan kajian kelengkungan untuk model struktur foil dalam penyelesaian serentak bearing lengkungan udara (FAB) rotor masalah dinamik. Kebanyakan kajian baru-baru ini di bearing lengkungan udara (FAB) rotor analisis dinamik telah terhad kepada model foil yang mudah di mana lengkungan individu telah dimodelkan sebagai bebas spring-peredam (ISD) subsistem. Dalam kajian ini, dinamik struktur foil lengkungan dikaji menggunakan teknik unsur (FE) dan teknik serentak mengira hasil daripada data. A model modal struktur foil penuh (FFSMM) dicipta dan kemudian diadaptasi ke dalam skim penyelesaian masalah FAB yang rotordynamic, bukan model ISD. Modal ini terhad kepada lima mod. Model pemutar-bearing juga disahkan terhadap keputusan eksperimen dan teori dalam kesusasteraan. Dari kajian ini, ia menunjukkan tidak ada kesan kelengkungan untuk model struktur foil benjolan. Ini kerana keputusan akhir sama dengan bukan kelengkungan atau linear model struktur foil benjolan. Tambahan pula, trajektori jurnal adalah sama dengan bentuk linear.

Penyelidik utama: Mohd Firdaus bin Hassan

E-mail: firdaus@ump.edu.my

Tel. No.: +609-4246250

Vote No.: RDU1703192

iv

ABSTRACT

This research is about study effect of curvature for modeling the bump foil structure in the simultaneous solution of foil-air bearing (FAB) rotor dynamic problems. Most recent research in foil-air bearing (FAB) rotor dynamic analysis has been limited to a simple bump foil model in which the individual bumps were modeled as independent spring-damper (ISD) subsystems. In these studies, the dynamics of the corrugated bump foil structure are studied using the finite element (FE) technique and simultaneous technique to calculate the result of the data. A full foil structure modal model (FFSMM) is created and then adapted into the rotordynamic FAB problem solution scheme, instead of the ISD model. A modal model is being limited into five modes. The rotor-bearing model is also validated against experimental and theoretical results in the literature. From this study, it showed there is no effect of curvature for modeling the bump foil structure. This is because the final result identical with the non-curvature or linear modeling the bump foil structure. Furthermore, the transient trajectory of the journal is identical with the linear form.

Key researchers: Mohd Firdaus bin Hassan

E-mail: firdaus@ump.edu.my

Tel. No.: +609-4246250

Vote No.: RDU1703192

TABLE OF CONTENT

APPENDIX B

LIST OF TABLES

LIST OF FIGURES

LIST OF SYMBOLS

$(\ )'$	differentiation with respect to τ
B	foil width (along z_f-axis)
c	undeformed radial clearance of FAB
D	diagonal damping matrix (eq. (9))
E	Young's Modulus
f_{res}	fundamental resonance of single isolated bump in Hz
f_p	vector of air pressure forces on bumps
F_x, F_y	Cartesian FAB forces
i, j	generic degrees of freedom
$\tilde{h}$	air film gap divided by c
H_{x_f}	foil modal matrix whose columns are $\phi_{x_f}^{(r)}, r = 1 \dots n_f$
H_{y_f}	foil modal matrix whose columns are $\phi_{y_f}^{(r)}, r = 1 \dots n_f$
k_{bump}	stiffness of single independent bump
K	FE stiffness matrix of foil structure
l_b	length of one bump along x_f-axis (Figure 2)
L	axial length of FAB
m_r	half-mass of rotor
M	FE mass matrix of foil structure
n_{bumps}	number of bumps
n_f	number of foil structure modes considered
N_z, N_θ	number of points of FD grid along ξ, θ directions
$p(\xi, \theta, \tau)$	absolute air pressure at (ξ, θ) for FAB
$p_a, \tilde{p}$	atmospheric pressure, p/p_a respectively
q_f	$n_f \times 1$ vector of modal coordinates

r	counter for foil modes
R	undeformed radius of FAB
$R_{x_f y_f}(0)$	static receptance matrix relating the elements in u with those in $-f_p$
$R_{y_f y_f}(0)$	static receptance matrix relating the elements in $-w$ with those in $-f_p$
S	static load in $-y$ direction
S_p	pitch of bumps (Figure 2)
t	time in seconds
t_b	thickness of foil
u	radius of rotor unbalance
$\boldsymbol{u}$	$n_{bumps} \times 1$ vector of the circumferential displacements at the bump apexes
w	foil deflection in radial direction
$\widetilde{w}$	$= w/c$
$\boldsymbol{w}$	$n_{bumps} \times 1$ vector containing the radial displacements at the bump apexes
x, y, z	Cartesian coordinate system (Figure 1)
x_J, y_J	Cartesian displacements of journal centre J relative to (fixed) bearing centre
x_f, y_f, z_f	Cartesian coordinate system local to the foil structure (Figure 2)
$\alpha_{ij}(\omega)$	receptance FRF relating generic degrees of freedom i and j
Δ	diagonal matrix of squares of foil natural circular frequencies
$\varepsilon_{x,y}$	$= x_J/c, y_J/c$
ε	$= \sqrt{\varepsilon_x^2 + \varepsilon_y^2}$
ξ	$= z_f/R$
ζ_{f_r}	viscous damping ratio of foil mode no. r

θ	angular local bearing coordinate (Figure 1)
$\phi_i^{(r)}$	mass-normalised modal displacement of foil in mode no. r at degree of freedom i
$\boldsymbol{\phi}_{x_f}^{(r)}$	$n_{bumps} \times 1$ mass-normalised eigenvector in mode no. r containing the circumferential displacements at the apexes of the bumps
$\boldsymbol{\phi}_{y_f}^{(r)}$	$n_{bumps} \times 1$ mass-normalised eigenvector in mode no. r containing the radial displacements at the apexes of the bumps
γ	attitude angle
Λ	bearing number [2, 3]
μ	air viscosity
ρ	density of foil material
η	damping loss factor of foil structure
$\psi(\xi, \theta, \tau)$	$= \tilde{p}\tilde{h}$
τ	non-dimensional time ($= \Omega t/2$)
Ω	rotational speed in rad/s
ω	general circular frequency in rad/s
ω_{f_r}	natural circular frequency of foil mode no. r in rad/s
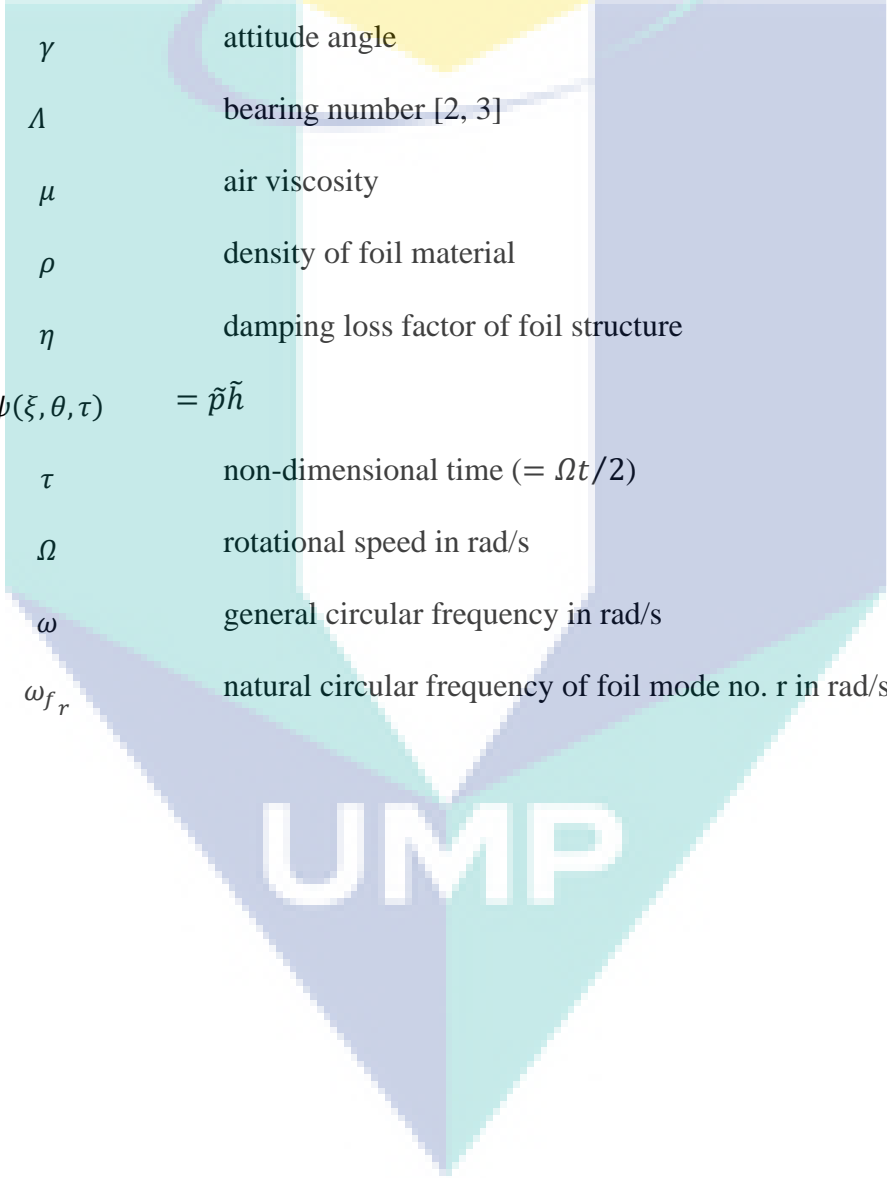
LIST OF ABBREVIATIONS

FFSMM   Full Foil Structure Model Modal

FEM   Finite Element Method

FVM   Finite Volume Method

FDM   Finite Differentation Method

ISD   Independent Spring Damper

ISDFM   Independent Spring Damper Foil Model
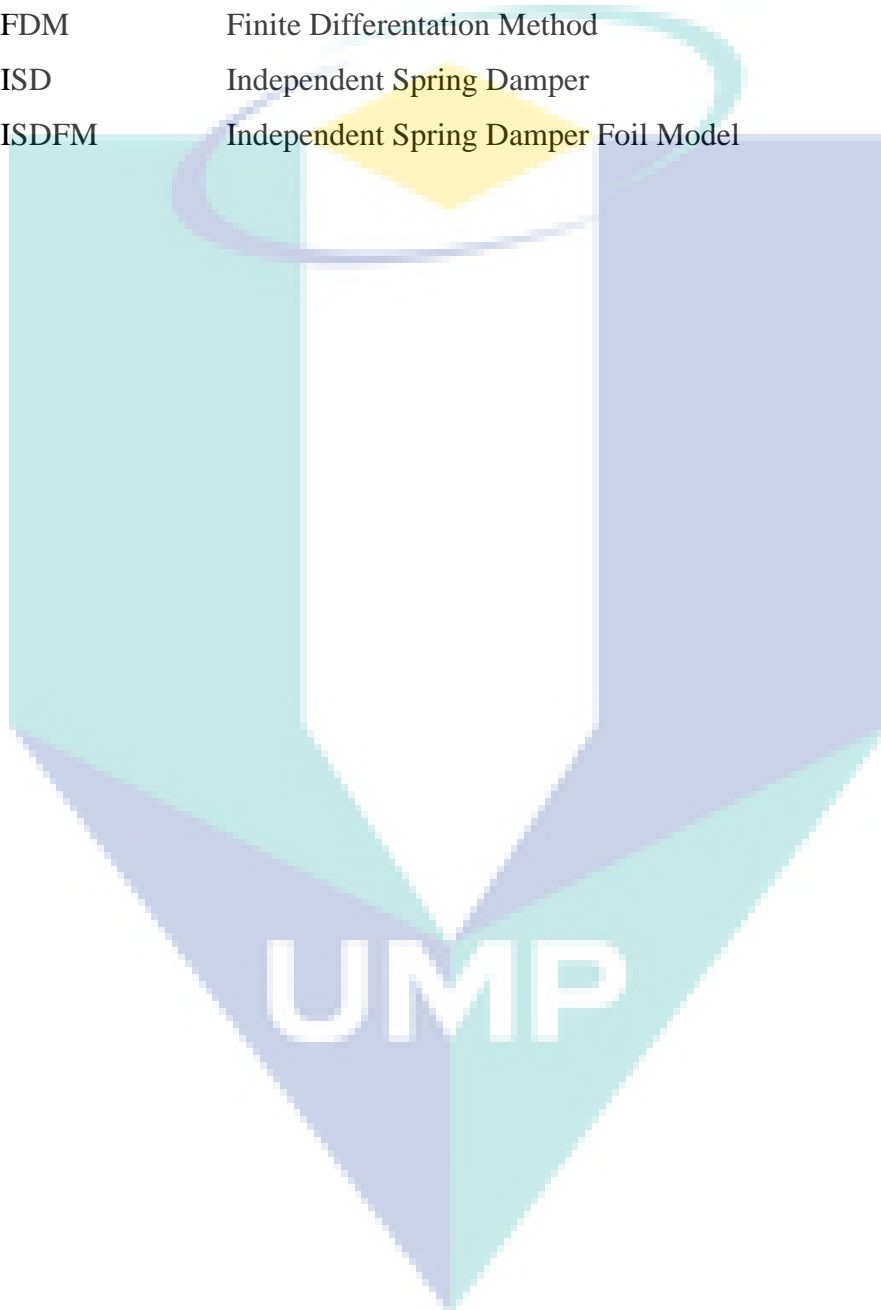
CHAPTER 1

INTRODUCTION

1.1   Introduction

The purpose of this chapter is to provide a review of this study. This chapter will described about the project background, problem statements, objectives and the overview about the study.

1.2   Project Background

Foil air bearings have made significant progress during the last 25 years. Reliability of many high speed turbomachines with foil bearings has increased over tenfold compared to those with rolling element bearings. Most recent research in foil-air bearing (FAB) rotor dynamic analysis has been limited to a simple bump foil model in which the individual bumps were modelled as independent spring-damper (ISD) subsystems. In these studies, the dynamics of the corrugated bump foil structure are studied using the finite element (FE) technique. A full foil structure modal model (FFSMM) is created and then adapted into the rotordynamic FAB problem solution scheme, instead of the ISD model. In this study, it will be shown that the fundamental frequency of corrugated structure with 26 bumps. The results using FFSMM foil model will be cross correlating for computing the deflection of the full foil structure.
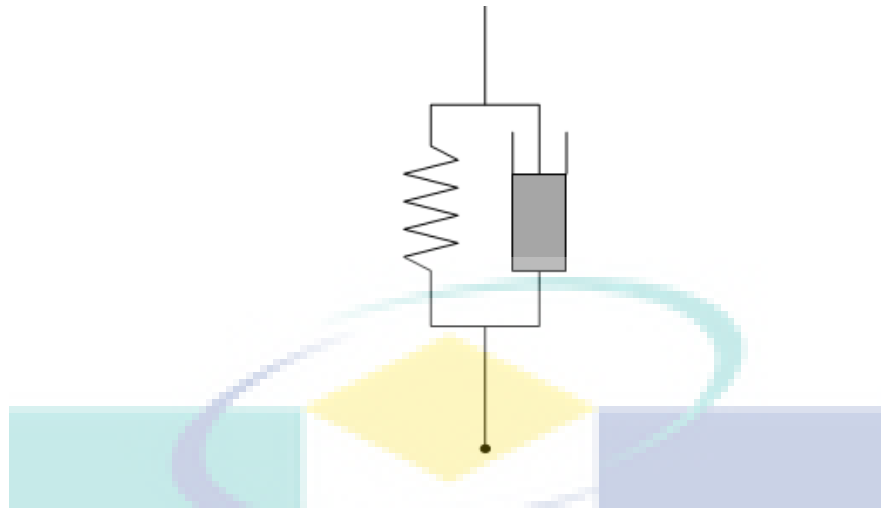
Figure 1.1:   Independent Spring-Damper (ISD) Subsystems

Source: Kim 2007
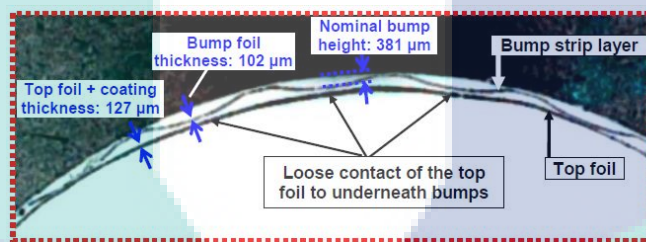
Figure 1.2:   Zoomed photo of Foil Air Bearing (FAB)

Source: Dissertation 2007

1.3   Problem Statement

Recent, FAB analysis has been limited to a simple bump foil model, independent spring damper (ISD).The study of ISD has only shown rotor dynamic analysis for a simple bump structure. Therefore, the effect of curvature for the modelling is going to discussed. The modal analysis of the bump foil structure into the simultaneous solution scheme is modelled or known as full foil structure modal model (FFSMM). The effect and the dynamic problems of the structure by performing finite element modal analysis were investigated.

1.4   Objectives of Study

In this study there are two main objectives. There are:

    i.   To investigate the effect of curvature to the dynamic behaviour (natural frequencies and mode shapes) of bump foil structure – 2D FE modal analysis.

    ii.   To apply the results in (1) to rotordynamic problem and discuss the significant of the curvature's effect.

1.5   Study Scopes

There are 4 main study scopes. There are:

    i.   Study and understand the concept of FAB.

    ii.   Design and perform the finite element analysis (FEA) of FAB using ANSYS® software.

    iii.   Analysis the data in MATLAB® based on formula.

    iv.   Inclusion of foil modal model into rotor-bearing problem.

CHAPTER 2

LITERATURE REVIEW

2.1 Introduction

The purpose of this chapter is to provide a review of past research efforts related to foil air bearing, generations and analyses methods and model of foil structure. A review of other relevant research studies is provided.

2.2 Foil Air Bearing (FAB)

Foil air bearings are compliant, self-acting hydrodynamic fluid film bearings which use air as their working fluid or lubricant[1]. A FAB supports the shaft by means of a cushion of air bounded by flexible foil structure. The introduction of the foil structure resolves the problems associated with the very tight radial clearance required by a plain air bearing. With a FAB, the hydrodynamic air film pressure generated as the shaft turns pushes the foil boundary away, allowing the shaft to become completely airborne [2]. As seen in the Figure 2.2, foil gas bearings consist of two parts, the smooth top foil and the corrugated bump foil [3]. As the shaft rotates, the pressure generated pushes the foil boundary away, allowing the shaft to become completely airborne [4]. Recent advances in foil air bearing design, finite element based rotor-dynamic analyses and high temperature solid lubrication provide the opportunity for new applications such as advanced oil-free turbomachinery [5]. The dynamics of FAB turbomachinery are governed by the interaction between the rotor, air films and the foil structures, and exhibit nonlinear effects [2]. Recent developments in foil bearing technology have heightened the need for a reliable and comprehensive compliant structure model to predict the behaviour of these bearings at a wide range of operating conditions [3].
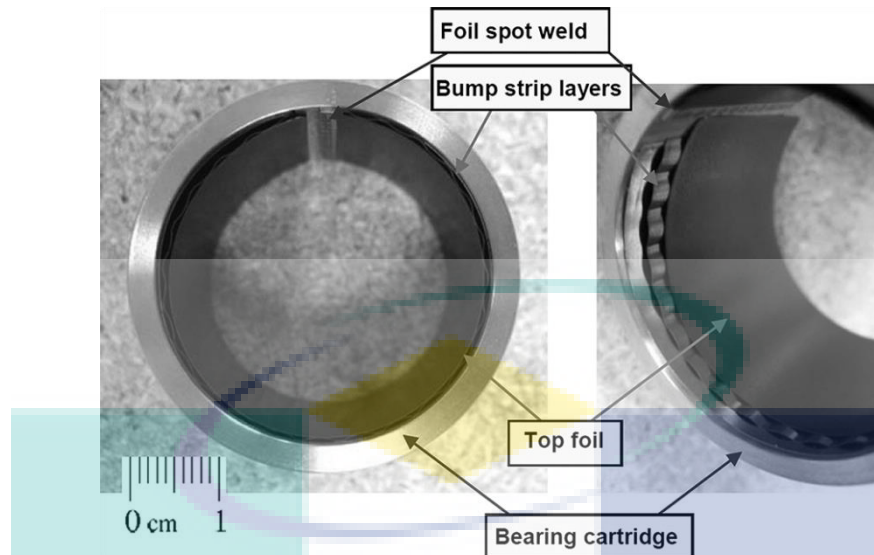
Figure 2.1:   Photo of Foil Bearing

Source Keun Ryu 2013
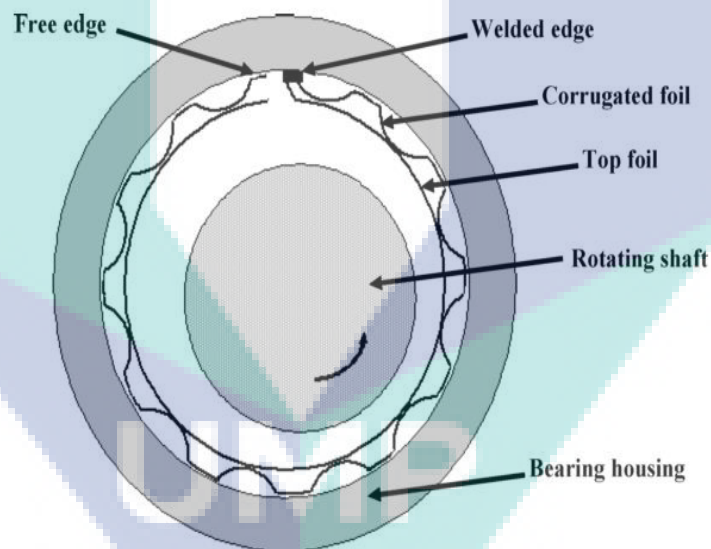
Figure 2.2:   Foil Air Bearing (Bump Types)

Source Le Lez 2008

2.3   Advantages and Applications

There a lots of advantages of FAB in turbomachinery that were discussed in others journal and researched. Firstly, FAB has higher reliability [6]. Foil bearing machines are more reliable because there are fewer parts necessary to support the rotative assembly and there is no lubrication needed to feed the system. When the machine is in operation,

the air film between the bearing and the shaft protects the bearing foils from wear. The bearing surface is in contact with the shaft only when the machine starts and stops. During this time, a coating on the foils limits the wear [7].

Secondly, FAB doesn't have scheduled for maintenance. There is no oil lubrication system in machines that use foil bearings, there is never a need to check and replace the lubricant. This results in lower operating costs [8].

Third, FAB is soft failure. This is because of the low clearances and tolerances inherent in foil bearing design and assembly, if a bearing failure does occur, the bearing foils restrain the shaft assembly from excessive movement. As a result, the damage is most often confined to the bearings and shaft surfaces. The shaft may be used as is or can be repaired. Damage to the other hardware, if any, is minimal and repairable during overhaul [9].

Besides that, FAB is environmental durability. Foil bearings can handle severe environmental conditions such as sand and dust ingestion. Large particles do not enter into the bearing flow path because of a reversed pitot design at the cooling flow inlet and smaller particles are continually flushed out of the bearings by the cooling flow. This ability to withstand contamination eliminates the need for filters in the airflow [10].

Furthermore, FAB can be operates in high speed machine. Compressor and turbine rotors have better aerodynamic efficiency at higher speeds. Foil bearings allow these machines to operate at the higher speeds without any limitation as with ball bearings. In fact, due to the hydrodynamic action, they have a higher load capacity as the speed increases [11].

FAB also capabilities operate in high and lower temperature. Many oil lubricants cannot operate at very high temperatures without breaking down. At low temperature, oil lubricants can become too viscous to operate effectively. Foil bearings, however, operate efficiently at severely high temperatures, as well as at cryogenic temperatures [6], [12].

Lastly, FAB also can involve in liquid operations. Foil bearings have been operated in process fluids other than air such as helium, xenon, refrigerants, liquid oxygen and liquid nitrogen. For applications in vapour cycles, the refrigerant can be used to cool

and support the foil bearings without the need for oil lubricants that can contaminate the system and reduce efficiency [7].

2.4   Concept and Generations of Foil Air Bearing (FAB)

There were three generation of foil air bearing. Generation I, Generation II and Generation III [13]. Generation I bearing is one in which the bump foil is axially and circumferentially symmetric. Generation II bump-type foil bearings take advantage of customizing the bump foil in either the axial or circumferential direction to alter the bearing's stiffness characteristics. Generation III bearings can be varied in the axial, radial, and circumferential directions to optimize performance [14]. Generation I was designs are characterized by having a uniform simple elastic foundation with uniform stiffness properties. The foil bearings exhibit load capacities approximately equal to rigid gas bearings of similar size [11]. Generation II foil bearings have a more complex elastic foundation in which the stiffness is tailored in one direction, for example, axially, to accommodate some environmental phenomena such as shaft misalignment or leakage of hydrodynamic fluid from the foil edges. These Generation II foil bearings exhibit load capacities approximately twice that of Generation I bearings [15]. Generation III foil bearings, with very complex elastic foundations, have stiffness that is tailored in two directions, often axial and radial. This level of design flexibility enables accommodation of edge effects and the ability to optimize bearing stiffness for varying loads. Generation III foil bearings have been shown to have load capacities three to four times greater than primitive Generation I bearings [16].
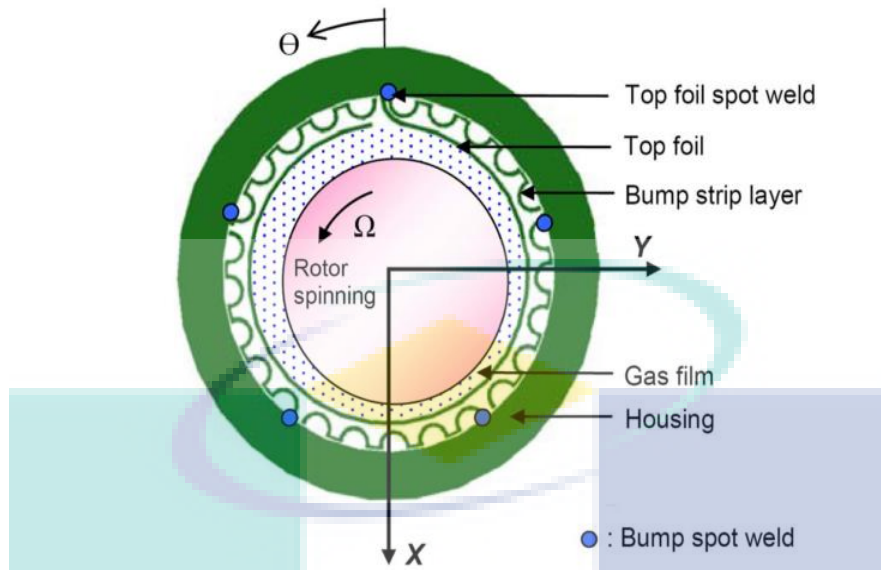
Figure 2.3:   Schematic of "second generation" bump type foil bearing

Source Kim 2014
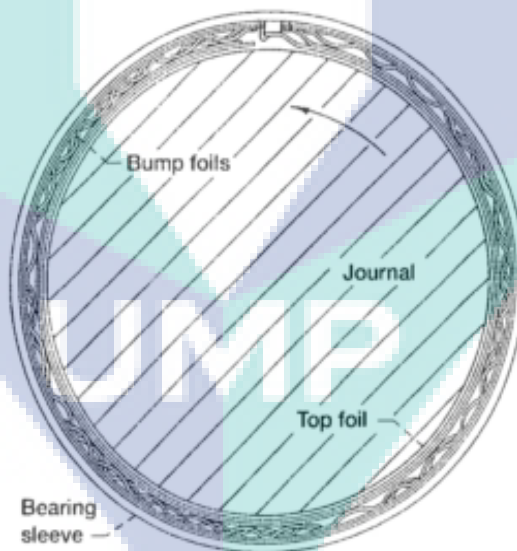
Figure 2.4:   Schematic of "third generation" bump type foil bearing

Source Howard 2002

8

The first-generation (Generation I) air foil bearing is analysed in this study [17]. Analyses of foil bearings require the simultaneous solution of structural deflection equations for the foil structure; usually the Reynolds equation for the gas film; and geometric equations relating the film thickness, the foil deflection, and the journal position [18]. Several different approaches have been used to solve this coupled system. The principle of an air or gas bearing is simple. As shown in Figure 2.5, when two surfaces form a wedge, and one surface moves relative to the other surface, pressure is generated between the surfaces due to the hydrodynamic action of the fluid which carries load [19], [20].

PRESSURE RISE

VELOCITY DISTRUBITION
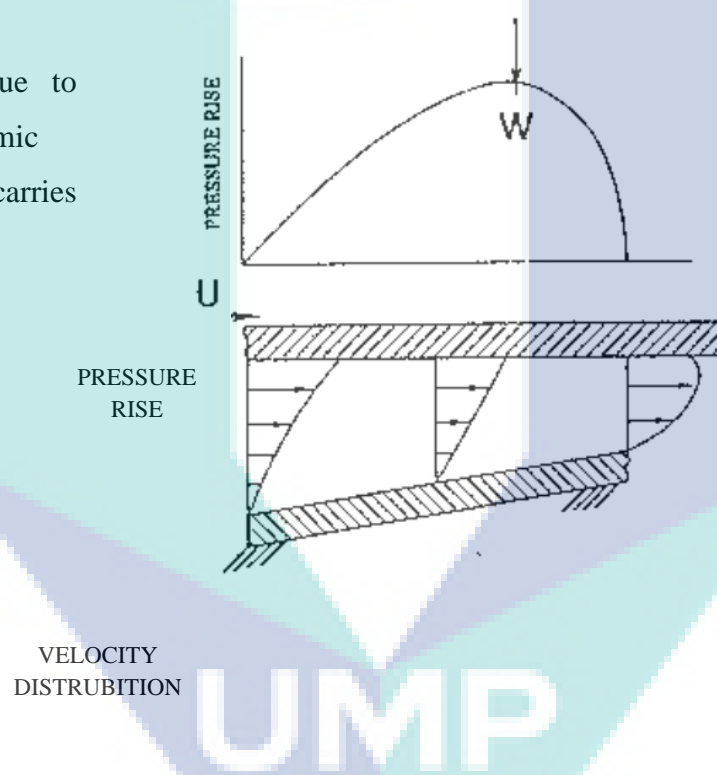
Figure 2.5:   Principle of an Air Bearing

Source Agrawal 1997

In a journal bearing, the shaft deflects and a wedge is formed due to the eccentricity between the shaft center and the bearing center. The resulting hydrodynamic pressure generation is shown in Figure 2.6. Even though, the principle of an air bearing is simple, application is complex [7].
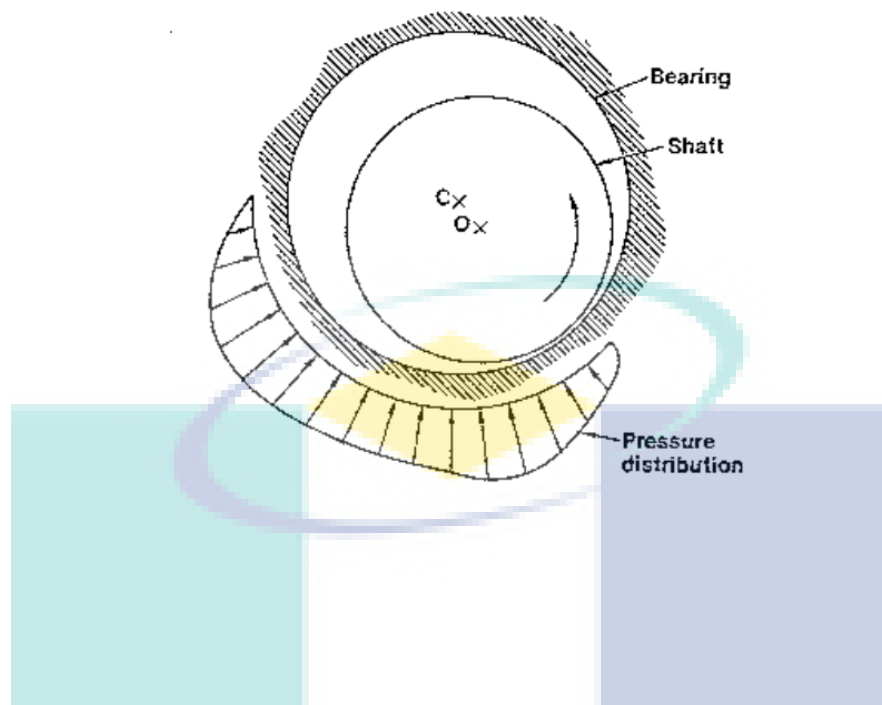
Figure 2.6:   Hydrodynamic Pressure
Generation

Source Agrawal 1997

According to some researches, when the shaft is running at 3600 rpm the radial clearance between the shaft and the bearing is less than 0.005 inch for a 2 inch diameter shaft. We can conclude that, damping is required to suppress any instability when work at various speed and temperatures. There also could be misalignment between the rotating parts and stationary parts. Foil bearing is the solved. When the shaft turns, a hydrodynamic pressure is generated which caused the shaft becomes completely airborne. The combination of hydrodynamic pressure with hydrostatic lift to circumvent the bearing wear issues during start/stops [21]. So, when the shaft is airborne, friction loss due to shaft rotation is small. As the shaft grows, the foils get pushed further away keeping the film clearance relatively constant. In addition, foils provide coulomb damping due to relative sliding, which is essential for stability of the machine. Various concepts of foil bearings have been tested.

2.5   Theoretical Analysis of FAB Rotor System

Several methods or solution have been presented to calculate the steady state characteristics of foil air rotor system. There are (i) Finite Element Method (ii) Finite

Volume Method and (iii) Finite Difference Method. These three methods can be used to solve Reynolds equation with arbitrary condition and numerical scheme[22].

2.5.1 Finite Element Method

Finite element method (FEM) will be focus in this study. FEM is numerical method for solving problem of engineering and mathematical physics. It is referred to as finite element analysis (FEA). In [23], an efficient finite element scheme for solving the non-linear Reynolds equation for compressible fluid coupled to compliant structures is presented. The method is general and fast and can be used in the analysis of air foil bearings with simplified or complex foil structure models. Simple elastic foundation model is applied to the analysis of a compliant foil air bearing to illustrate the computational performance. In this paper the scheme is faster and it state that it is not only for steady-state analysis but also for non-linear time domain analysis of rotor supported by air foil bearings. In this paper the FEM is divided into two parts. The first part is focused on dealing with the zero-order non-linear parabolic partial differential equations for the static pressure p_0 which need to solve iteratively while the second part deals with the first-order linear complex differential equations for the dynamic pressure, p.

In [24], a finite element model is used to describe the foil elasticity. It is performed between the Reynolds equation, the foil elastic deflection equation and the energy equation until it archived convergence. In paper [25], the analysis of gas foil air bearings is integrating FE top foil models. The paper introduces two finite element models for the top foil elastic structure. The simplest FE model assumes the top foil as a 1D thin beam-like structure with negligible deflections along the axial coordinate and acted upon by a uniformly distributed pressure field. The second FE model, 2D, takes the top foil as a flat shell.

2.5.2 Finite Volume Method

Finite volume method (FVM) is a method for representing and evaluating partial differential equations in the form of algebraic equations. The method is similar with finite difference method or finite element method, the values are calculated at discrete places on a meshed geometry. Arghir et al. paper's [26] presented a finite volume solution where the pressure was implicitly integrated for a prescribed gap perturbation to calculate linear

stiffness and damping coefficients dependent on the perturbation amplitude. The numerical solution was developed for the general case when the film thickness can have discontinuities and was formulated in the frame of the finite-volume method applied on unstructured grids. In [27], finite-volume method based on the finite difference method was applied for the numerical simulation which uses no orthogonal coordinates.

2.5.3   Finite Difference Method

Finite difference method (FDM) are numerical methods for solving differential equations by approximating them with difference equations which finite differences approximate the derives. FDM is discretization methods. In [22] , the paper develop the use of Chebyshev polynomial fits to identify the FD solution of the incompressible Reynolds equation. It manipulates the Reynolds equation to allow efficient and accurate identification in the presence of cavitation, the feed-groove, feed-ports, end-plate seals and supply pressure. It is the first FD models were developed. Chebyshev identified bearing models are shown to mimic accurately and consistently the simulations obtained from the FD models[28].

Among others researched, Wang and Chen's paper [29] used finite difference for the spatial and temporal dimensions when solving the Reynolds equation. They simulated the steady-state response of a perfectly balanced rigid rotor supported by two identical bearings. The spatial discretisation was performed with a central-difference scheme, while the temporal discretisation was performed with an implicit-backward-difference scheme.

2.6   Model of Foil Structure

The structure of the FAB is simple and easy. The leading edge of the top foil is free, whereas the trailing edge is typically welded to the bearing sleeve [30]. In Abdelrasoul M. Gad and Shigehiko Kaneko papers [31], they were adopted several assumptions in their analysis. There are the displacement of the bumps is from the fixed end towards the free end, the top foil is a thin deformable plate that follows the bump foil deflection and does not deflect relative to bumps, all deformations are elastic and no permanent deformation occurs, the bump ends do not separate from the rigid bearing surface, however the flat segment between bumps may deflect laterally and since the

bump ends are rigidly attached to the flat segment between bumps, the boundary condition at both bump ends is assumed initially to be rigid support.
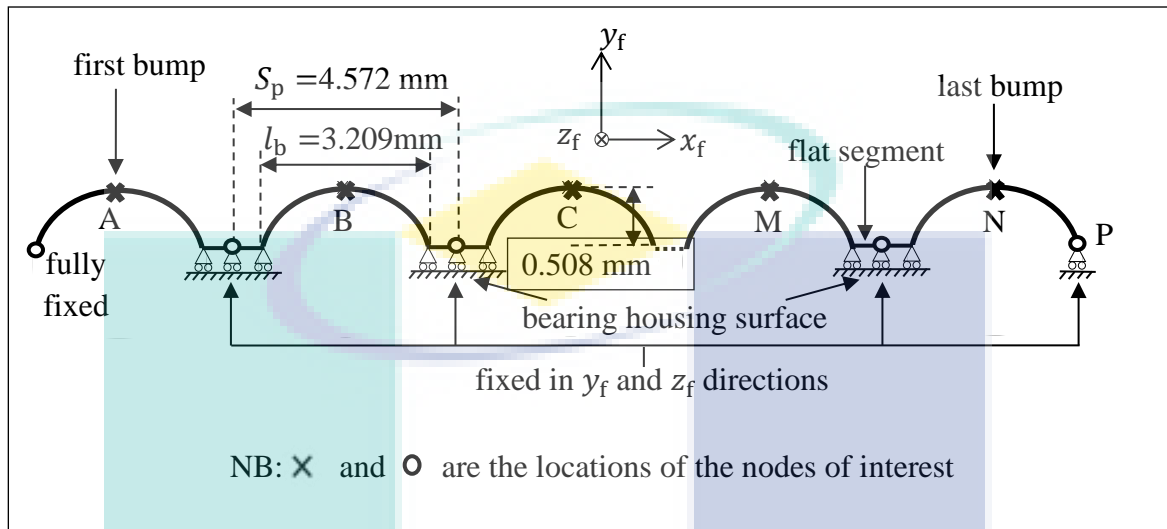
Source Hassan 2016

Figure 2.7: Bump foil dimensions

In Figure 2.7, we can see that the left hand edge is fully welded and right hand edge constrained only in the y and z direction. The structure in Figure 2.7 has the same geometry in most of paper or studies [4], [10], [32]. The width B of the bump (along z axis) is equal to the bearing length L. The $x_f z_f$-plane, which corresponds to the bearing housing surface, is taken to be a flat plane. The curvature of the bearing shell is neglected). This assumption is reasonable because the ratio between the heights of the bump strip layer to the radius of the bearing is very small. Hence, the longitudinal (x_f) direction corresponds to the circumferential direction of the bearing and the transverse (y_f) direction corresponds to the radial direction of the bearing.

Table 2.1: Geometry and materials of the bump-type foil bearing

Number of bumps	26
Thickness, t_b	0.102 mm
Bearing radius, R	19.05 mm
Bearing length, L	38.1 mm
Measured radial clearance, C_m^a	31.8 µm
Bump pitch, s_0	4.572 mm
Bump height, h_b	0.508 mm
Young's modulus, E	214 GPa
Bump foil Poisson's ratio, v	0.29
Density, p	7850 kg/m^3

Source: Feng 2010

2.7 Solution Techniques

For solution technique of FAB, there are two types. There are non-simultaneous solution technique and simultaneous solution technique. Both of the technique had been done by many researched. But for this study, the focus is on simultaneous solution technique.

2.7.1 Simultaneous Solution Technique

In [33], it show on how to solve the three main equations simultaneous in the time domain. There are two methods used which are Finite Difference (FD) and Galerkin Reduction (GR). For FD method, the RE is discretized on a grid of N_z x N_0 points. These are the three main equations.

$$\psi' = \frac{1}{\Lambda}\left\{\frac{\partial}{\partial\theta}\left[\psi\left(\tilde{h}\frac{\partial\psi}{\partial\theta} - \psi\frac{\partial\tilde{h}}{\partial\theta}\right)\right] + \frac{\partial}{\partial\xi}\left[\psi\left(\tilde{h}\frac{\partial\psi}{\partial\xi} - \psi\frac{\partial\tilde{h}}{\partial\xi}\right)\right]\right\} - \frac{\partial\psi}{\partial\theta}$$

2.1

$$\frac{dw(\theta)}{d\tau} = \frac{2}{\eta}\left(\frac{F}{K} - w(\theta)\right)$$

2.2

$$\varepsilon_x'' = \frac{4}{m_r c\Omega^2}(F_x + m_r u\Omega^2\cos 2\tau), \quad \varepsilon_y'' = \frac{4}{m_r c\Omega^2}(F_y + S + m_r u\Omega^2\sin 2\tau)$$

2.3

These three main equations Eq. 2.1, Eq. 2.2 and Eq. 2.3 are then transformed into system of ordinary differential equation with the state variables.

But for second method, Galerkin Reduction (GR) method is a mesh-free transformation (i.e. it involves no physical spatial discretisation) and therefore has the potential of considerably reducing the number of state variables[4]. GR was detail briefly in [34] which show to calculate the stability of static equilibrium solution of a rotor system with air bearings. However, most of researched doesn't not use this method cause the prohibitive workload involved in evaluating the huge number of analytical integrals in the GR residual functions. In GR the Resynolds Equation is expressed as:

$$\psi = \bar{h} + \varphi \qquad\qquad 2.4$$

where is a approximated by a truncated Fourier series in the two partial coordinates. The Galerkin's method then is applied to minimize the approximation error, with the base functions being used as the weighting factor.

2.8   Development of Foil Air Bearing (FAB)

Ku and Heshmat presented an analytical mathematical bump foil model [35]. Hesmat originally included the flexibility of the foil structure in the Reynolds equation by introducing a linear elastic displacement as function of the fluid film pressure, $h_c = K(p - pa)$ based on the work of Walowit and Anno [36]. Walowit and Anno were first introduced a theoretical model for a single bump to determine its deflection under load. This model assumed that bumps do not interact with each other, thus neglecting local interactive forces between bumps as well as friction forces between the top foil and the bumps. It was a 2D model in which the bending and tensile stiffness of a bump were considered. According to this model, when the top foil is loaded, each bump has identical stiffness   and deflection [37]. This work was a first step toward understanding the frictional forces between compliant element contact surfaces and local interacting forces in bump foil strips and, more importantly, their effects on both local and overall stiffness and damping characteristics of the foil bearings [38].

In 1992, Ku and Heshmat developed a theoretical model for determining the deformation of the bump foil under a given load distribution [14]. A theoretical model of

the foil structure with the consideration of the friction forces and the local interaction forces of bumps was presented to predict the coulomb stiffness and damping. The curvature effect of journal bearings was also appended in the following published research work [39]. Hesmat was using the 2D model to the hydrodynamic lubrication theory to evaluate thrust and journal gas bearing performance [38]. According to [40], a comprehensive computer program was developed to determine deflections, stiffness, displacement, and reacting and friction forces for each bump in a bump foil strip. In addition to variable geometric parameters, the program enables the computation of equivalent friction coefficients and overall stiffness of a bump foil strip under various load distributions. The main result of this investigation was that the bumps near the fixed end exhibit much higher stiffness than those near the free end. Higher friction coefficients tend to increase stiffness and may pin down bumps near the fixed end. In addition, the load distribution profile and bump configuration greatly influence bump foil stiffness. This body of work is now available to be used as a design guide for improving the performance of compliant foil bearings.
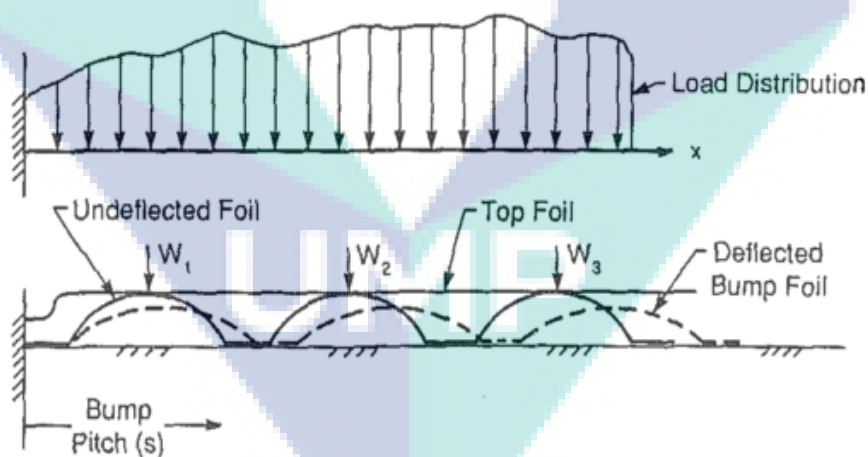
Figure 2.8:   Bump foil strip with and without applied load

Source Rani 2013

16

DellaCorte and Valco developed a simple empirical based method for approximating bearing loads for various types of foil bearings over a range of speeds. The bearing load capacity is related to the bearing diameter, axial length of the bearing and rotor speed by the empirical design dependent load capacity coefficient [14]. DellaCorte presented a rule of thumb (ROT) based analytical formula predicting comparative load capacities of various air foil bearings and provided design guidelines for the air foil bearings [41]. The ROT is developed as an aid in feasibility assessments for foil bearing supported rotordynamic systems [42]. ROT enables simplified load capacity estimation for foil air journal bearings and can guide development of new oil free turbomachinery systems. DellaCorte introduced simple equations, derived from previously published empirical data, to estimate the stiffness and damping coefficients of foil bearings for early design stage use. The stiffness and damping equations are functions of stiffness and damping coefficients and the bearing projected area, with a range of suggested coefficients. Simple calculations such as these are incredibly useful during the early bearing design stages [14].

Peng and Carpino also present an analytical method of calculating bearing stiffness and damping coefficient using a linear perturbation method as a function of the bump compliance parameter [43]. They are the first introduced the concept of an equivalent viscous damping of the foil structure. They treated the foil structure as spring damper systems as shown in Figure 2.9 [44]. They calculated the damping coefficient of the bump foil using the equivalent viscous damping derived from the energy dissipation principles. And they calculated the dynamic characteristics using these damping components. In that study, the equivalent viscous damping for the Coulomb damping was calculated by equating the energies dissipated in a cycle of journal excitation. They verified that this equivalent viscous damping component makes the overall stiffness and damping of the bump foil bearing increase [45]. They said in the study the stiffness and the damping coefficients of the bearing increase as the Coulomb friction increases [46].
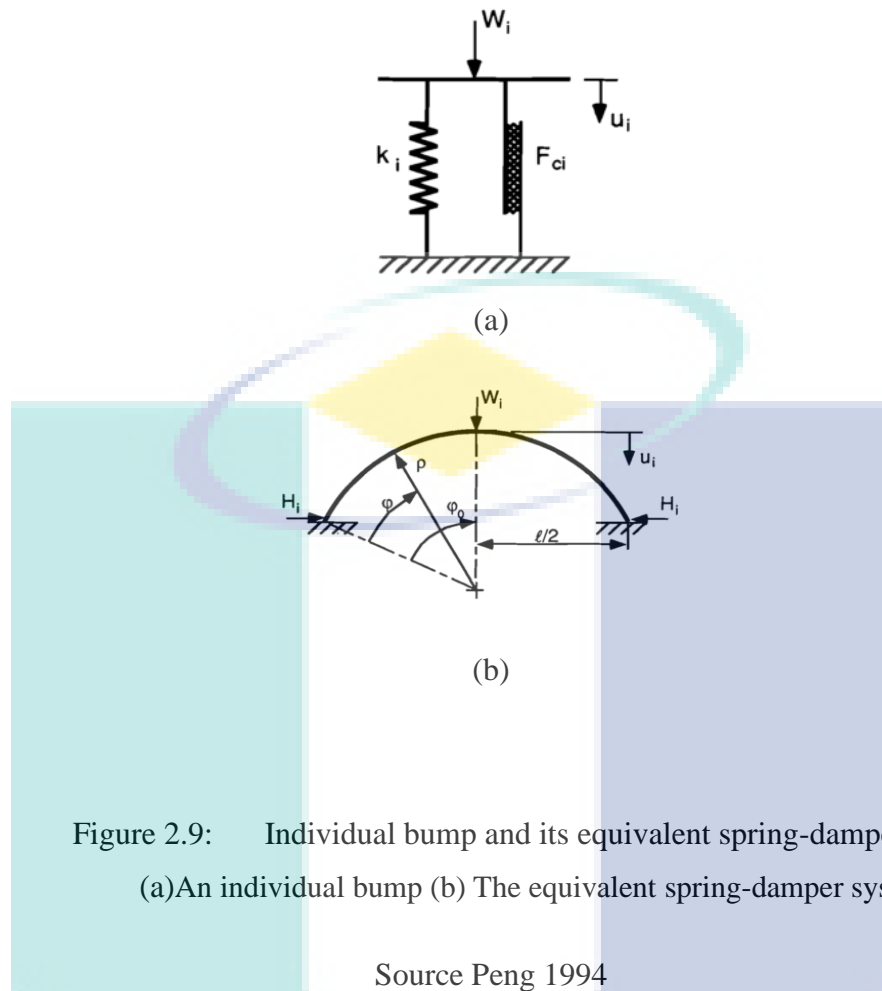
Figure 2.9:   Individual bump and its equivalent spring-damper system

(a)An individual bump (b) The equivalent spring-damper system

Source Peng 1994

From Figure 2.9(a) above, when the top of the bump is pushed further down from the equilibrium position, the direction of H_i will be toward the centre of the bump to resists the deflection. When the force is released H_i will be in the direction away from the bump centre. The calculation can be seen in [46]. Each bump is analogous to a spring-damper system as shown in Figure 2.9(b), where k is the spring constant and F_c is the Coulomb damping force per unit area.

Carpino and Talmage presented a fully coupled finite-element formulation, taking into consideration the membrane and bending effect of the top foil and the radial and circumferential deflections of the bump foil with the effect of Coulomb friction between the top foil, the bumps, and the housing[10]. A single four noded finite element that incorporates the elastically supported shell structure of the foil and the gas film modelled by a compressible Reynolds equation is developed. The resulting system of nonlinear finite element is solved by the Newton Raphson method [18]. From this system, we

predict pressure and film thickness distributions, load capacity, and torque for a typical foil bearing.

In Le Lez et al. paper [47] an analytical model of the whole corrugated sheet has been presented. In these study Le Lez et al. presented a model using three elementary springs to replace each bump as shown in Figure 2.9. Therefore, the friction forces between foils could be considered as loads at the top point of each bump. Then, Le Lez et al. modified this method to take into account the dry friction within foils and presented a nonlinear numerical model to predict the stability and unbalanced response [14], [47]. However, the resonance computed by Le Lez et al in [48] was based on a single independent bump, rather than the whole foil structure.
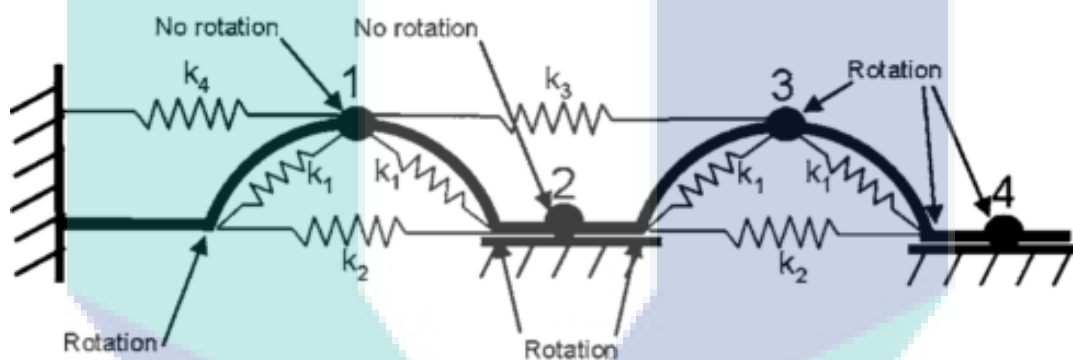
Figure 2.10:   A model using three elementary springs to replace each bump

Source Le Lez 2007

In the present paper, it will be shown that the fundamental frequency of a corrugated structure with 26 bumps similar to that in [49] is typically almost five times less (1.9 kHz). Another work has incorporated an FE model of the bump foil structure, including its inertia, into the rotor-bearing problem [50], but ignored bump curvature, and is computationally cumbersome for simultaneous solution of the rotor-air-foil domains since it does not involve any modal reduction.

CHAPTER 3

METHODOLOGY

3.1   Introduction

The purpose of this chapter is to provide a review of this study's methodology. This chapter will described about the finite analysis in ANSYS® software, execute program in MATLAB® software and inclusion of foil modal model into rotor bearing problem.

3.2   Finite Analysis in ANSYS Software

Finite analysis is performed using ANSYS® Mechanical. The analysis is performed using 2-dimensional (2D) elements (beam). In ANSYS®, BEAM188 is being selected which is a linear (2-node) beam element. After consider the parameters in ANSYS®, keypoint is generated with the assists of MATLAB®. There are 304 keypoints were generated from the MATLAB® to form a complete 26 bumps. Figure 3.1 showed the complete design of the FAB.
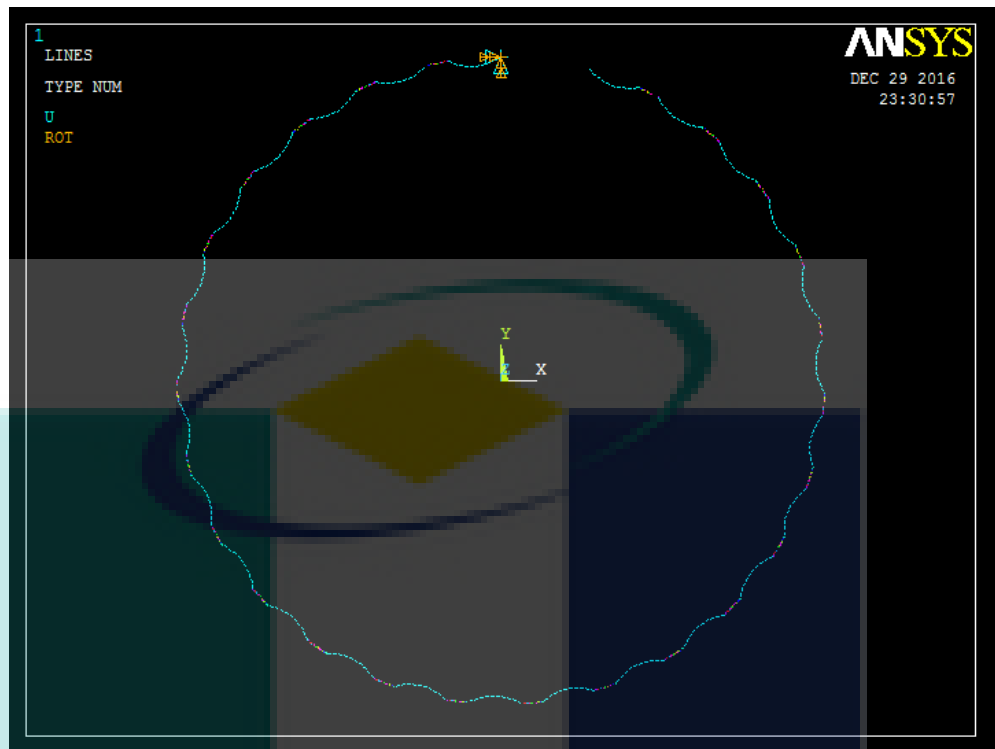
Figure 3.1:   A complete 26 bumps of FAB in ANSYS®

In Figure 3.1, at the first (first keypoints) which in the left-hand it constraints to all directions, xf, yf and zf direction since the points is welded to the bearing sleeve while on the end of the bearing, the right-hand edge constrained only in the yf and zf direction. For the flat segment, there were 10 keypoints to join to form a straight line which equal to 3.209 mm. The length of the bump and the flat surface is same as shown in Figure 2.7. The flat segments was fixed in y_f and and z_f directions as the flat segment is corresponds to the bearing housing surface. There were only 3 keypoints on the flat segments were constraints because the distance to each other is small and it does no effect the result and the design as shown in Figure 3.3. The constraints of the complete FAB showed in Figure 3.2.
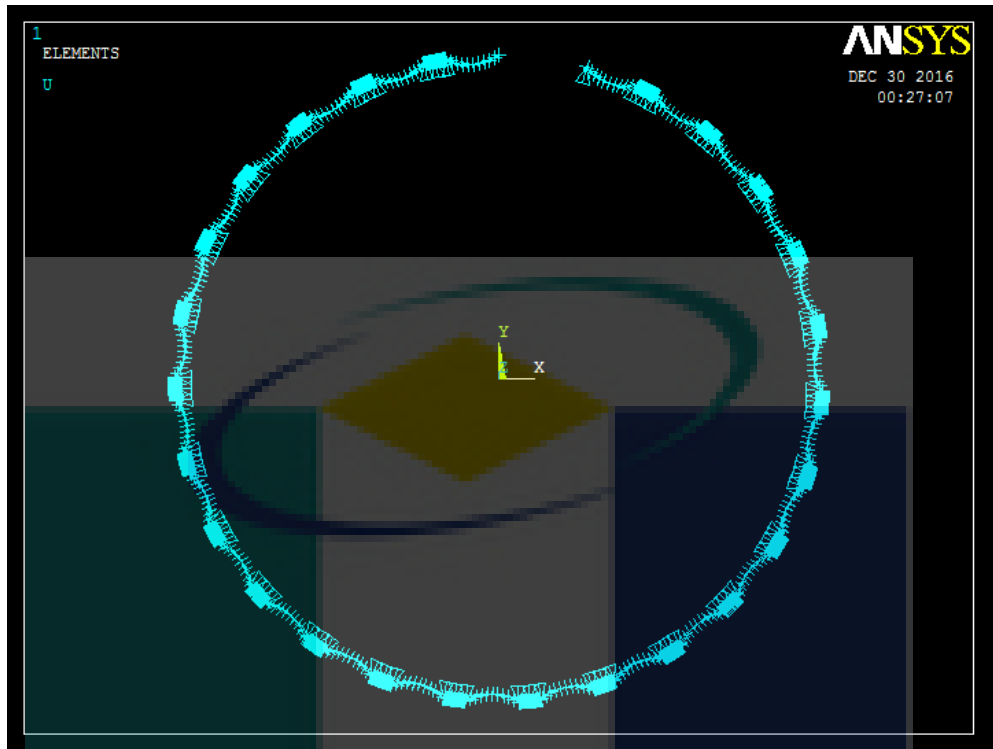
Figure 3.3:   The FAB was constrain
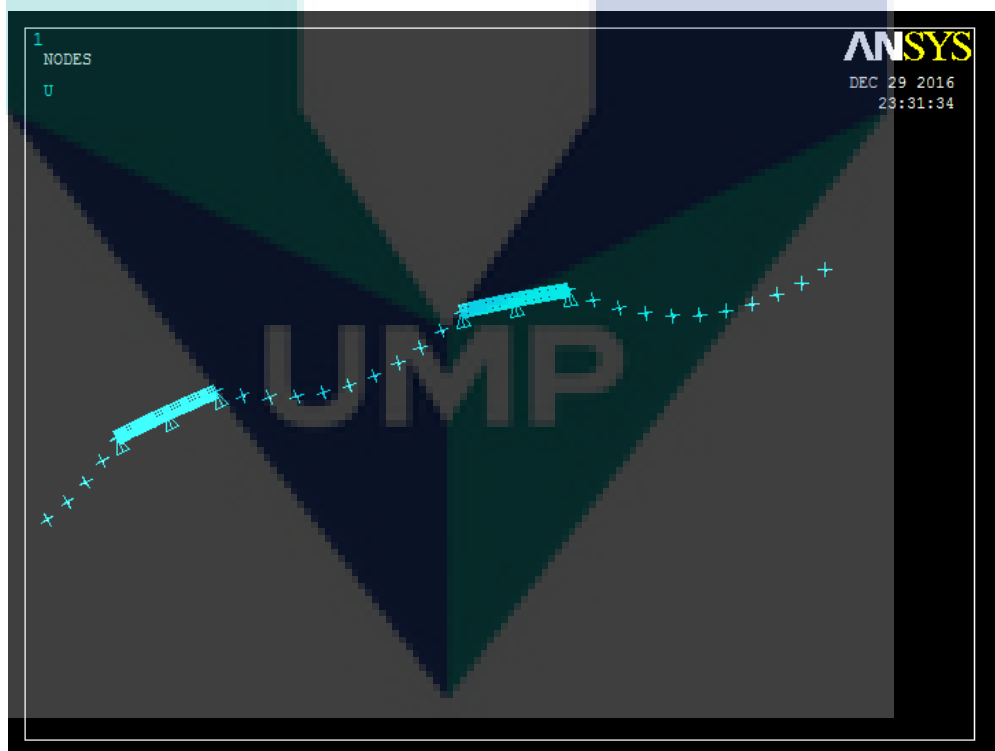
Figure 3.2:   The flat segments were constraints to y_f and z_f direction while the bump is constraints to z_f direction only

The system is analyzed for two case, free vibration (modal analysis) and forced vibration (harmonic response). Modal analysis is the study of the dynamic properties of structures under vibrational excitation while harmonic analysis is used to predict the steady state dynamic response of a structure subjected to sinusoidal varying loads. In ANSYS®, modal analysis is used to determine a structure's vibration characteristics, natural frequencies and mode shapes. In this study, the number of mode to extract is set to 300 to make the frequency more accurate. Table 3.1 showed some of the mode and the frequency that was run on ANSYS® for modal analysis.

Table 3.1:   Some of modes were extracted by ANSYS from 300 modes

SET	TIME/FREQ	LOAD	STEP	SUBSTEP
1	2227.2	1	1	1
2	5395.7	1	2	2
3	6147.7	1	3	3
4	6148.3	1	4	4
5	6149.2	1	5	5
6	6150.5	1	6	6
7	6152.1	1	7	7
8	6154	1	8	8
9	6156.3	1	9	9
10	6158.8	1	10	10
11	6161.5	1	11	11
12	6164.5	1	12	12
13	6167.6	1	13	13
14	6170.8	1	14	14
15	6174.1	1	15	15
16	6177.4	1	16	16
17	6180.7	1	17	17
18	6183.9	1	18	18
19	6187.1	1	19	19
20	6190.0	1	20	20

From the complete data of the 300 number modes, it showed that the value of frequency almost similar to each other. For this study, five natural frequencies were being

selected by using harmonic analysis. In ANSYS®, harmonic analysis is used to determine the response of the structure under a steady-state sinusoidal (harmonic) loading at a given frequency. Harmonic analysis can verify which one of the natural frequencies can overcome resonance, fatigue and other harmful effects of forced vibrations. Figure 3.4 below showed one of the natural frequency that being select based on amplitude graph in harmonic analysis. Table 3.2 showed the five natural frequencies that being selected after the harmonic analysis.
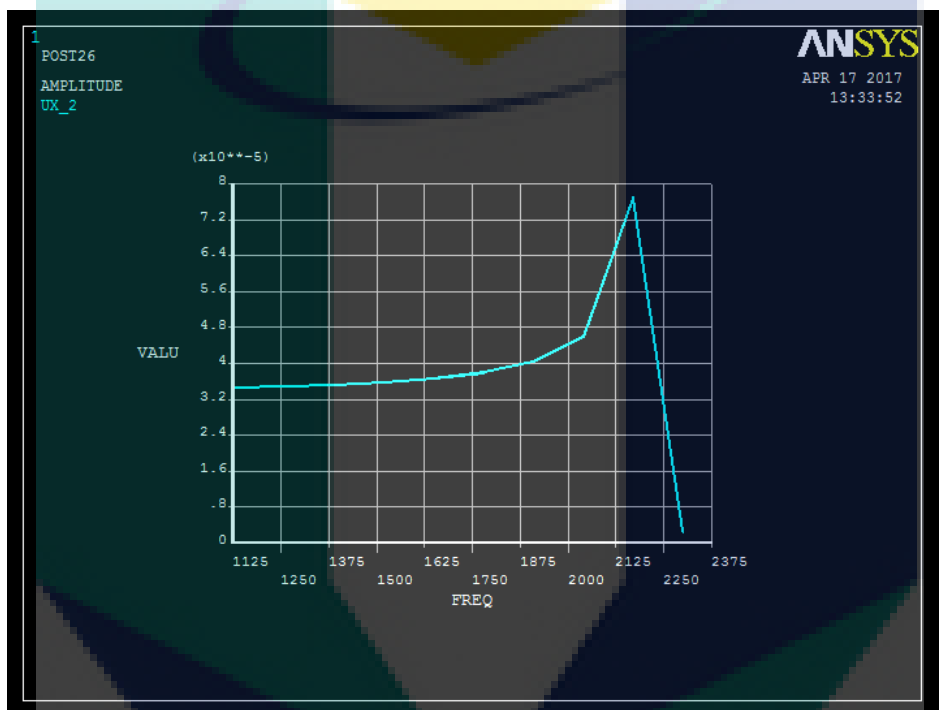
Figure 3.4:   Highest value of natural frequency in amplitude graph in range of 1125 Hz to 2376 Hz which is 2227.2 Hz for the first modeshape.

Table 3.2:   Five natural frequencies of foil structure computed by FE in 2760 elements after harmonic analysis

Modeshape	Set	Natural frequencies in Hz
1	1	2227.2
2	28	6620.2
3	81	10836
4	183	14780
5	211	18384

These five natural frequencies (eigenvalues) can produce different animation of the bumps and modeshape (eigenvectors). Figure 3.5, Figure 3.6, Figure 3.7, Figure 3.8

and Figure 3.9 showed the animation of the bump based on different natural frequency. Different natural frequency produced different modeshape.
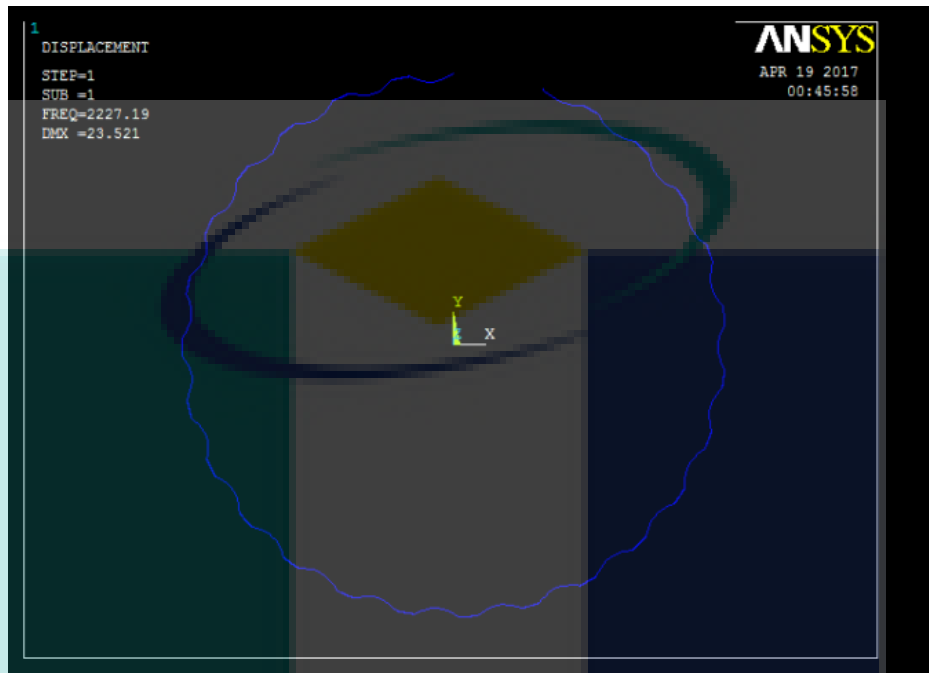
Figure 3.5: The animation in ANSYS® for the first natural frequency, 2227 Hz
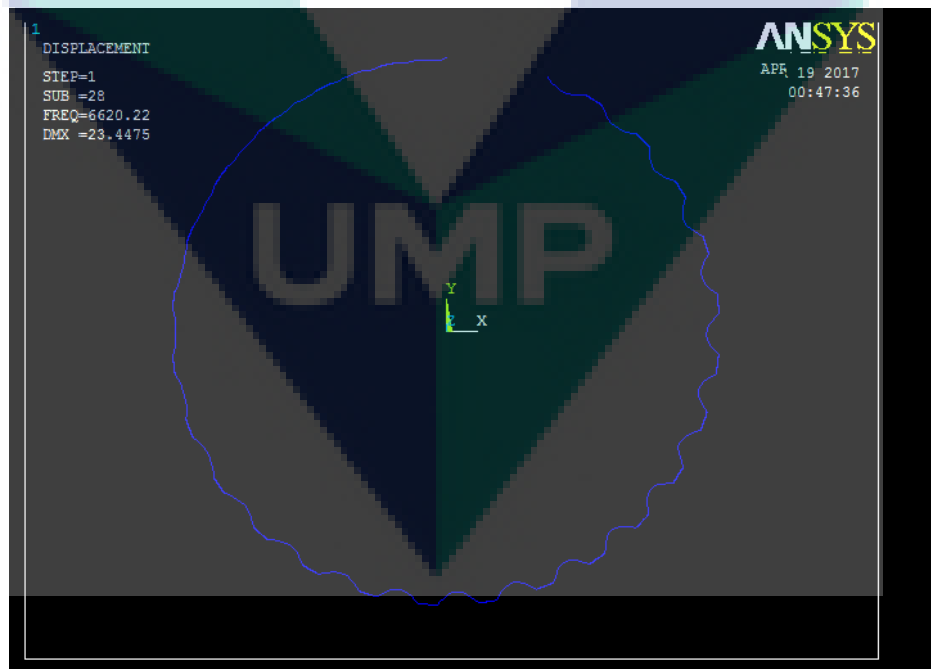
Figure 3.6: The animation in ANSYS® for the second natural frequency, 6620.2 Hz
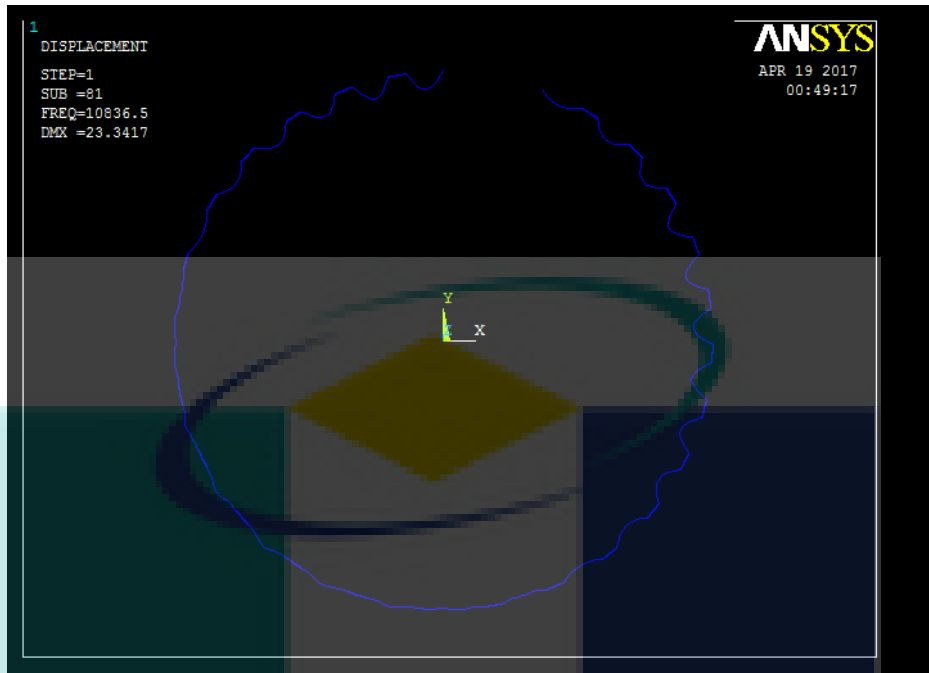
Figure 3.7: The animation in ANSYS® for the third natural frequency, 10836 Hz
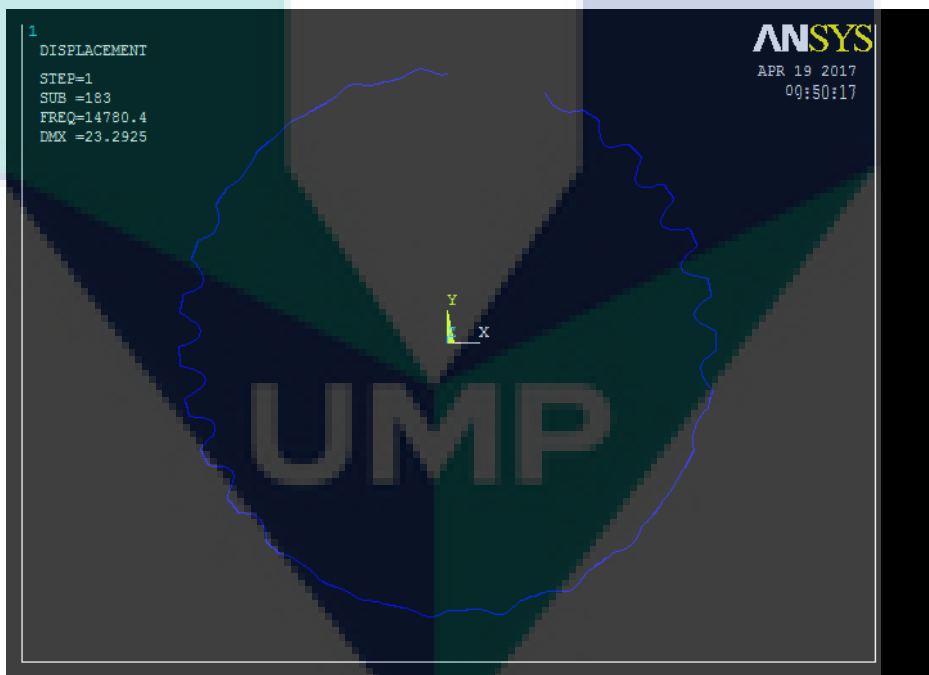
Figure 3.8: The animation in ANSYS® for the fourth natural frequency, 14780.4 Hz
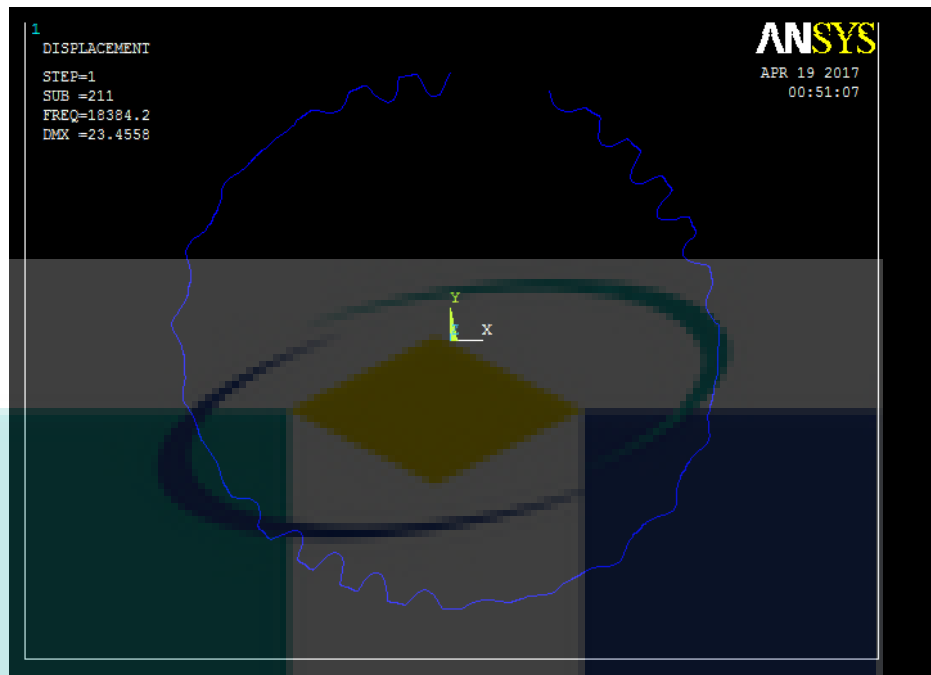
Figure 3.9:   The animation in ANSYS® for the fifth natural
frequency, 18384.2 Hz

3.3   Execute Program In MATLAB® Software

From the Figure 3.5 to Figure 3.9 before in Section 3.2, each of the natural frequency generated 2761 nodes of modeshape for x and y axis. For this study, there are about 26 bumps and not all nodes were study for some reason. For x axis, the focus is modeshape on the centre of the flat segments while for the y axis is modeshape on the centre of the bump as seen in Figure 3.10 below. As seen in Figure 2.10 in Chapter 2, the crosses refer to the apex points (centre of the bumps) and the circles refer to the midpoints of flat segments between the bumps, and the fixed and free edges (centre of the flat segments). So a coding had been made in MATLAB® programming to calculate the modeshape and generate the required 26 modeshape. Then generate graphs according to the modeshape as shown in Figure 3.11, Figure 3.12, Figure 3.13, Figure 3.14, and Figure 3.15. There are two graphs that were generated by the MATLAB®. Transverse vibration graph is for the modeshape on y_f while longitudinal vibration on x_f.
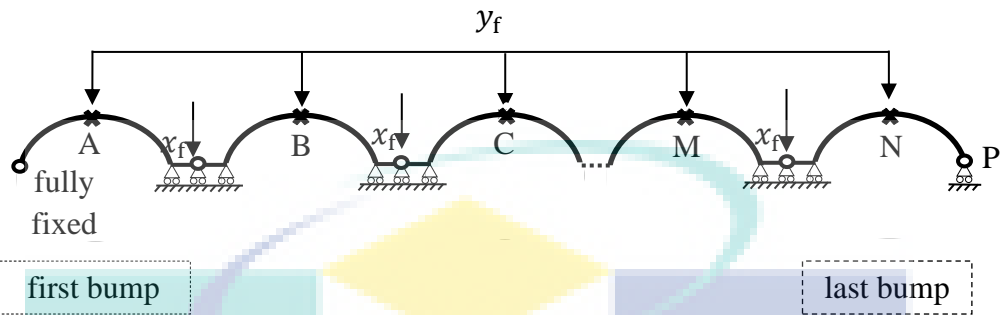
Figure 3.10:   The points of modeshape that were study and been calculated in MATLAB® coding
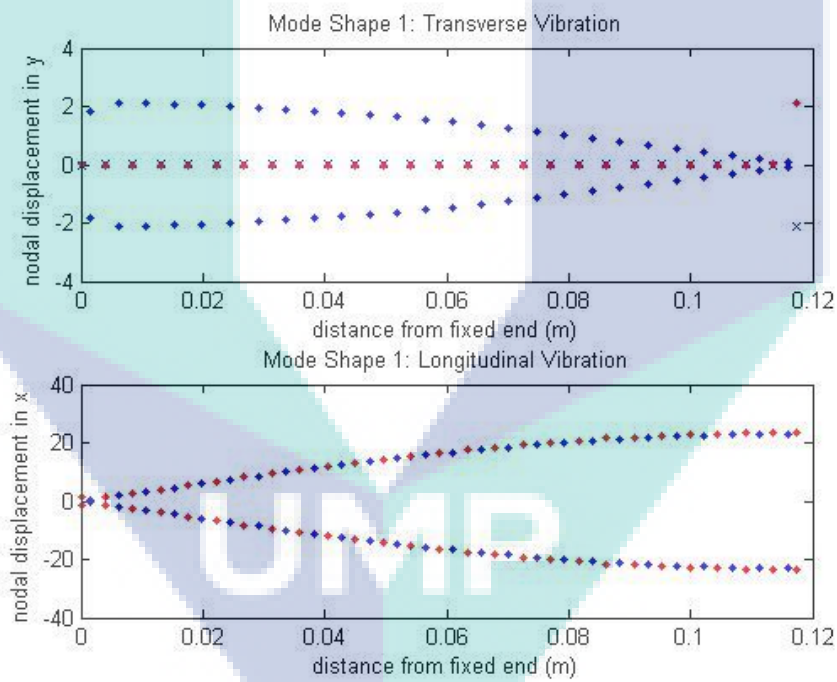
Figure 3.11:   First mode shape of the bump foil structure, computed using 2D FE (beam elements)
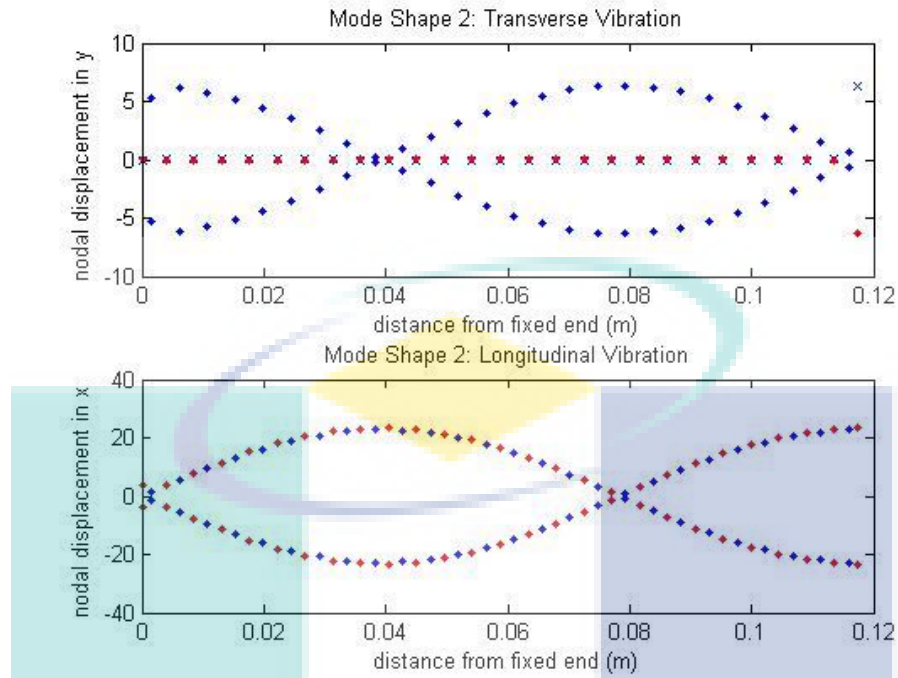
Figure 3.12: Second mode shape of the bump foil structure, computed using 2D FE (beam elements)
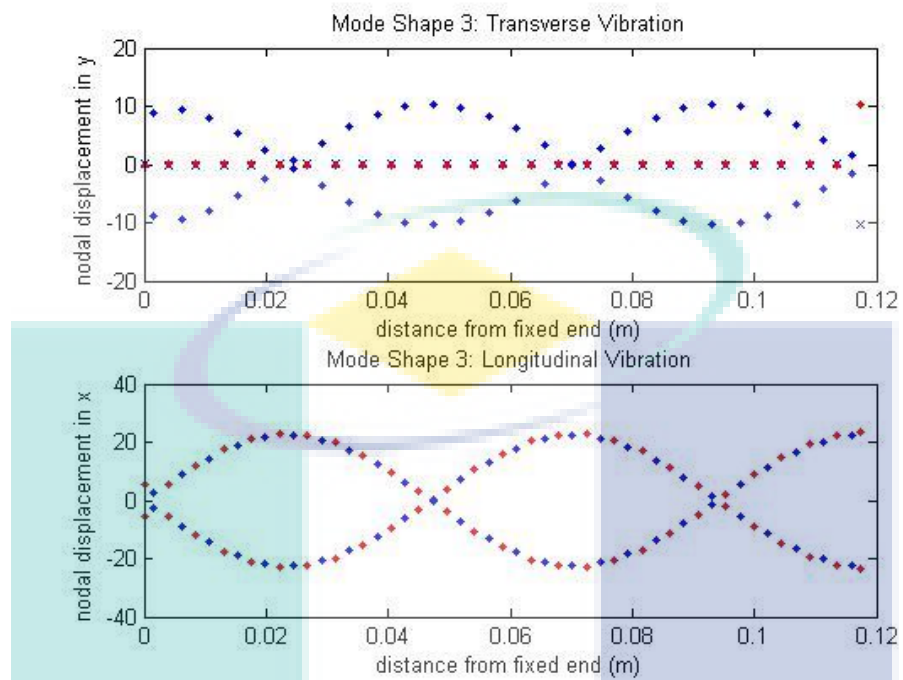
Figure 3.13:   Third mode shape of the bump foil structure, computed
using 2D FE (beam elements)
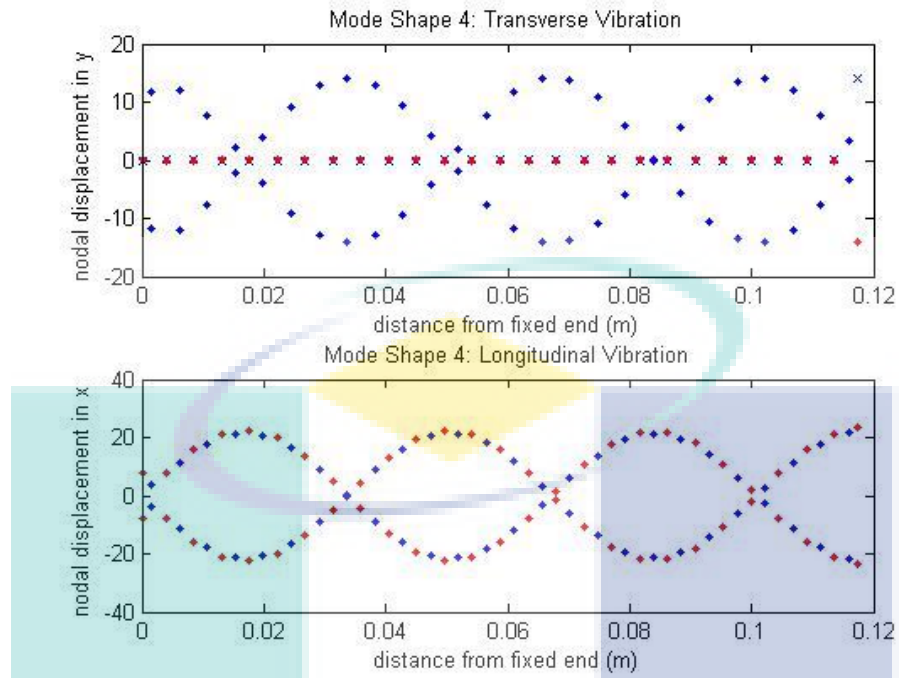
Figure 3.14:   Third mode shape of the bump foil structure, computed
using 2D FE (beam elements)
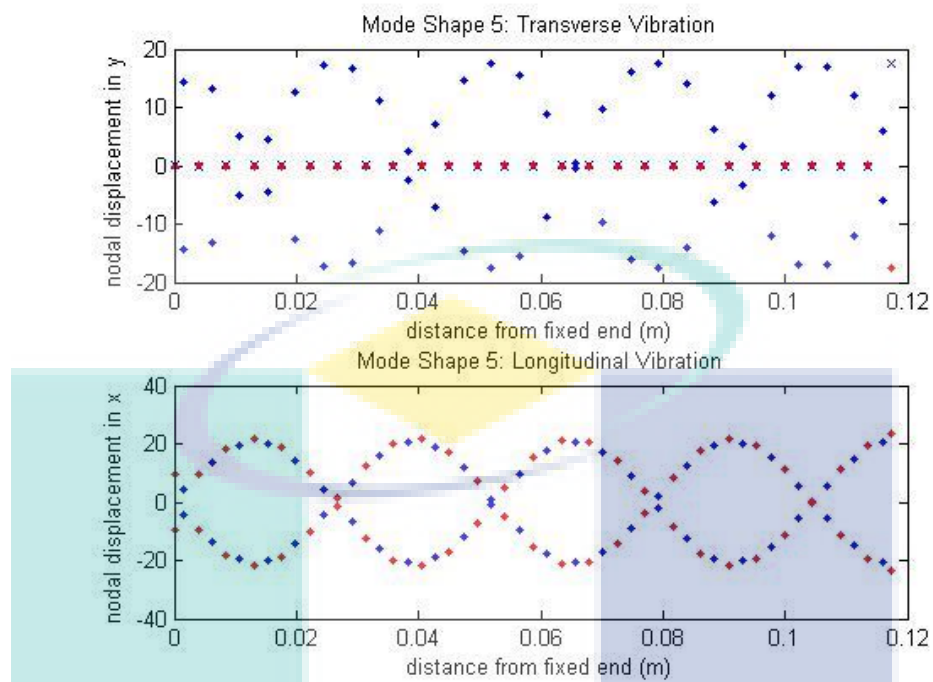
Figure 3.15:   Fifth mode shape of the bump foil structure, computed
using 2D FE (beam elements)

Figure 3.16 showed the 26 values of apex points, $\mathbf{H_{y_f}}$ (modeshape) for all five natural frequencies. These values of the modeshape will be used to calculate radial displacement, w. The equation to calculate it will be discussed in Chapter 4. Besides that, to calculate the final result simultaneous solution was been used and will be discussed details in Chapter 4.
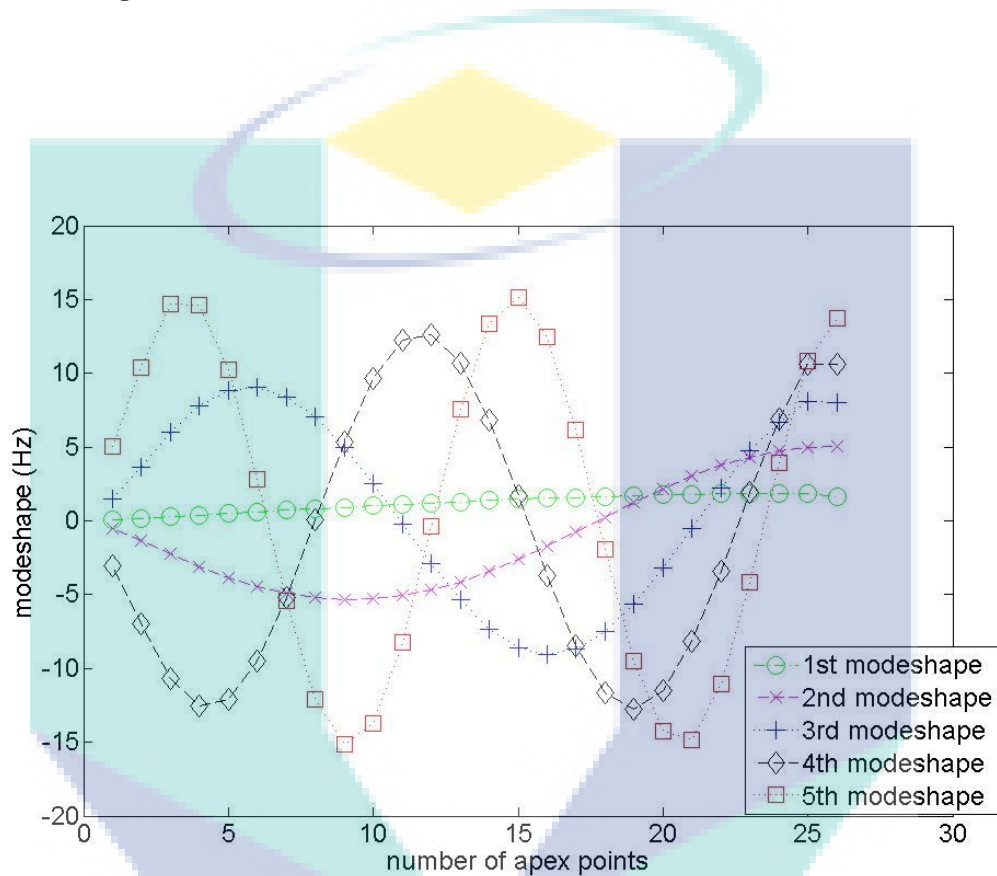
Figure 3.16:   Modeshape values (H_{y_f}) for all 5 natural frequencies

CHAPTER 4

RESULTS AND DISCUSSION

4.1   Introduction

The purpose of this chapter is to provide a review of this study's result. This chapter will described about the inclusion of foil modal model into rotor bearing problem, the results of FAB simultaneous rotor solution and validation of rotor-bearing model against published results.

4.2   Inclusion of Foil Modal Model into Rotor Bearing Problem
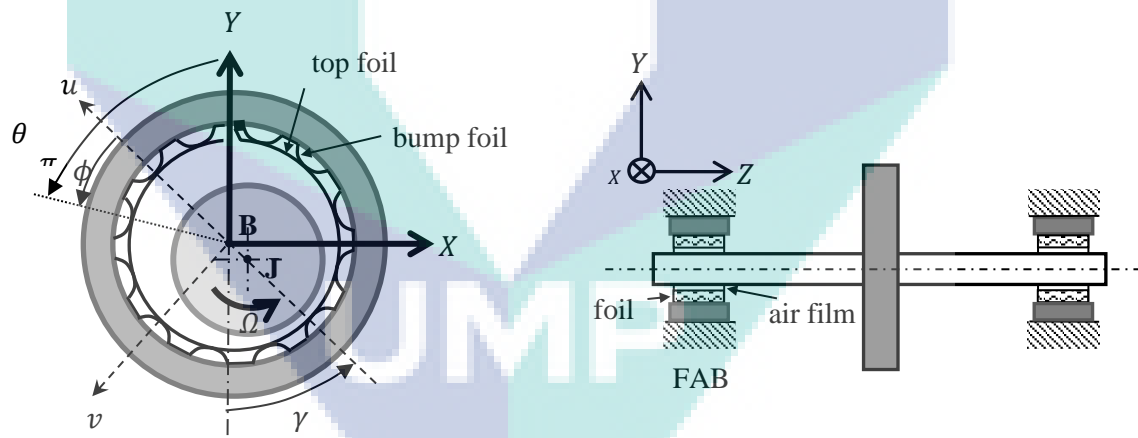
Figure 4.1:   FAB and symmetric rigid rotor FAB system

Source Hassan 2016

From Figure 4.1, equations governing the translational motion of the symmetric rigid rotor-FAB system [5], [51] with rotor of mass m_r per bearing rotating with angular velocity Ω and subjected to a static load S in the y direction can be written as:

$$\varepsilon_x{}'' = \frac{4}{m_r c \Omega^2} (F_x + m_r u \Omega^2 \cos 2\tau), \quad \varepsilon_y{}'' = \frac{4}{m_r c \Omega^2} \left(F_y + S + m_r u \Omega^2 \sin 2\tau \right) \qquad 4.1$$

where: $\tau = \Omega t/2$ is the non-dimensional time and $(\ )'$ denotes $\partial(\ )/\partial\tau$, $\varepsilon_x = x_J/c$, $\varepsilon_y = y_J/c$ are the displacements of the journal J in the x, y directions (relative to the bearing centre B, which is assumed to be fixed) normalized by the radial clearance c (which is the air gap when the journal is centralized in the bearing with no foil deflection), S is the static load in the y direction per bearing $(= -m_r g$, in this work), and u the unbalance eccentricity. F_x and F_y are the air-film reaction forces on the journal, obtained by integrating the air film pressure distribution over the bearing area.

In [4], [5], a pressure function is governed by the isothermal Reynolds Equation (RE) in equation 4.2 below. For a FAB of radius R and length L (Figure 4.1), let $p(\xi, \theta, \tau)$ denote the air film pressure (absolute) where $\xi = \frac{z_f}{R}$.

$$\psi' = \frac{1}{\Lambda} \left\{ \frac{\partial}{\partial \theta} \left[\psi \left(\tilde{h} \frac{\partial \psi}{\partial \theta} - \psi \frac{\partial \tilde{h}}{\partial \theta} \right) \right] + \frac{\partial}{\partial \xi} \left[\psi \left(\tilde{h} \frac{\partial \psi}{\partial \xi} - \psi \frac{\partial \tilde{h}}{\partial \xi} \right) \right] \right\} - \frac{\partial \psi}{\partial \theta} \qquad 4.2$$

where: Λ is the bearing number, $\psi = \tilde{p}\tilde{h}$, $\tilde{p} = \frac{p}{p_a}$, p_a being the atmospheric pressure and $\tilde{h}$ the non-dimensional air-film gap at a position (ξ, θ) [2, 3]:

$$\tilde{h} = 1 - \varepsilon_x \cos\theta - \varepsilon_y \sin\theta + \tilde{w}$$

$$4.3$$

$\tilde{w} = \frac{w}{c}$ being the non-dimensional foil deflection in the radial direction at a position (ξ, θ). As in [49], [52], [53], and as justified by the agreement between the 2D and 3D FE mode shapes in Figure 2.7, it shall be assumed that the variation of the foil deflection in the axial (z_f) direction is negligible, meaning that $\tilde{w}$ is a function of θ only. For given θ, $\tilde{w}$ is obtained by interpolation from the $n_{bumps} \times 1$ vector $\mathbf{w}$ containing the radial displacements at the apexes of the bumps. It is proposed that $\mathbf{w}$ can in principle be expressed as a superposition of n_f bump foil structure modes:

$$\mathbf{w} = -\mathbf{H_{y_f}}\mathbf{q_f}(\tau), \mathbf{H_{y_f}} = \begin{bmatrix} \boldsymbol{\phi}_{\mathbf{y_f}}^{(1)} & \cdots & \boldsymbol{\phi}_{\mathbf{y_f}}^{(n_f)} \end{bmatrix}$$

4.4

where $\mathbf{q_f}$ is the $n_f \times 1$ vector of modal coordinates, $\mathbf{H_{y_f}}$ is the value of apex points that get in Chapter 3. It is noted that the elements in $\boldsymbol{\phi}_{\mathbf{y_f}}^{(r)}$ are positive in the $+y_f$ direction (see Figure 2.7), whereas the elements in $\mathbf{w}$ are positive when radially outward (corresponding to the $-y_f$ direction). $\mathbf{q_f}$ is governed by the modal equations of the bump foil structure (expressed in terms of the non-dimensional time τ):

$$(\Omega^2/4)\mathbf{q_f}'' + (\Omega/2)\mathbf{D}\mathbf{q_f}' + \Delta\mathbf{q_f} = -\mathbf{H_{y_f}^T}\mathbf{f_p}$$

4.5

where $\mathbf{f_p}$ is the $n_{\text{bumps}} \times 1$ vector of air pressure forces on the bumps, obtained by averaging $p(\xi, \theta, \tau)$ over a bump projected area of $S_p \times L$. $\mathbf{D}$ and Δ are the diagonal matrices:

$$\mathbf{D} = \mathbf{diag}[\cdots \quad 2\zeta_{f_r}\omega_{f_r} \quad \cdots], \Delta = \mathbf{diag}[\cdots \quad \omega_{f_r}^2 \quad \cdots]$$

4.6

It is noted that, in this preliminary work, friction forces in the circumferential (x_f) direction (see Figure 2.7) are not considered, but their equivalent damping effect is accounted as equivalent viscous damping in the matrix $\mathbf{D}$, where ζ_{f_r} is the viscous damping ratio of mode no. r (as done in the case of spring-damper foil models, which used a loss factor e.g.[46].

MATLAB® coding had been done to calculate the full foil structure modal model (FFSMM) in the simultaneous solution for five modes. It was calculated using 3 main equations. There are original modal superposition equation for the foil deflection, Eq. 4.3, pressure function, Eq. 4.2 and radial displacement, Eq.4.4. In the coding, the mass of the bearing, $m_r = 3.061$ kg, bearing radius $R = 19.05$ mm, bearing length $L = 38.1$ mm, $p_a = 101325$ Pa, air viscosity $\mu = 1.95 \times 10^{-5}$ N/m^2 , loss factor value of $\eta = 0.25$ and the undeformed foil clearance $c = 32 \times 10^{-6}$ m were being constant. The static load per bearing in the y-direction $S = -m_r g$. The values of N_z and N_θ in the

solution are 7 and 72 respectively. N_z and N_θ are number of points of FD grid along ξ, θ directions.

Figure 4.2 showed the result of transient trajectory of journal over constant shaft revolution and constant value of mass balance, $m_r u = 0$ but in different value of rpm. FFSMM solution also had been run in different value of mass balance, $m_r u$ as shown in Figure 4.3 and Figure 4.4. The solution showed from initial conditions corresponding to zero journal centre displacements and velocity, air film at atmospheric pressure and undeformed foil.
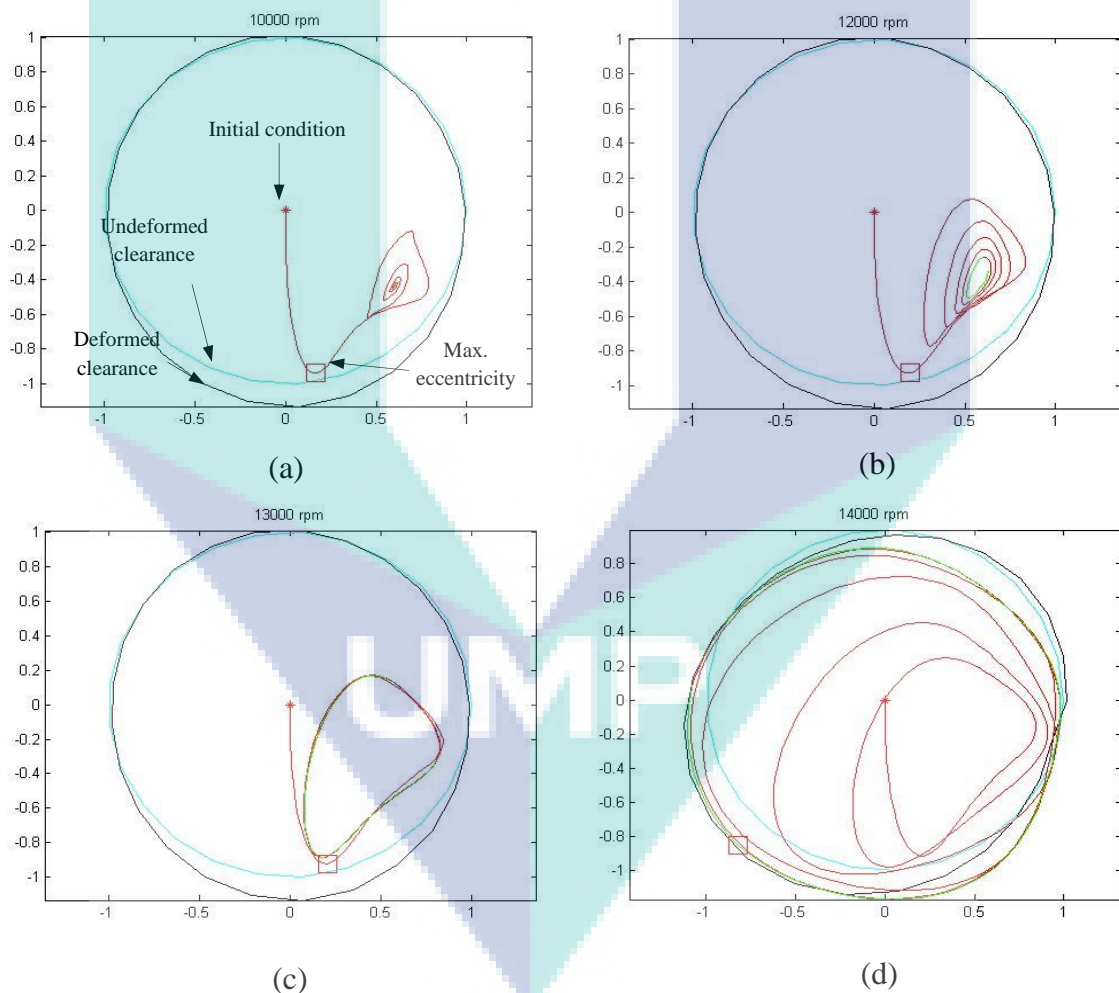
Figure 4.2:   Transient journal trajectory over 12 revs with $m_r u = 0$ g.mm at (a) 10,000 rpm; (b) 12,000 rpm; (c) 13,000 rpm; (d)14,000 rpm.
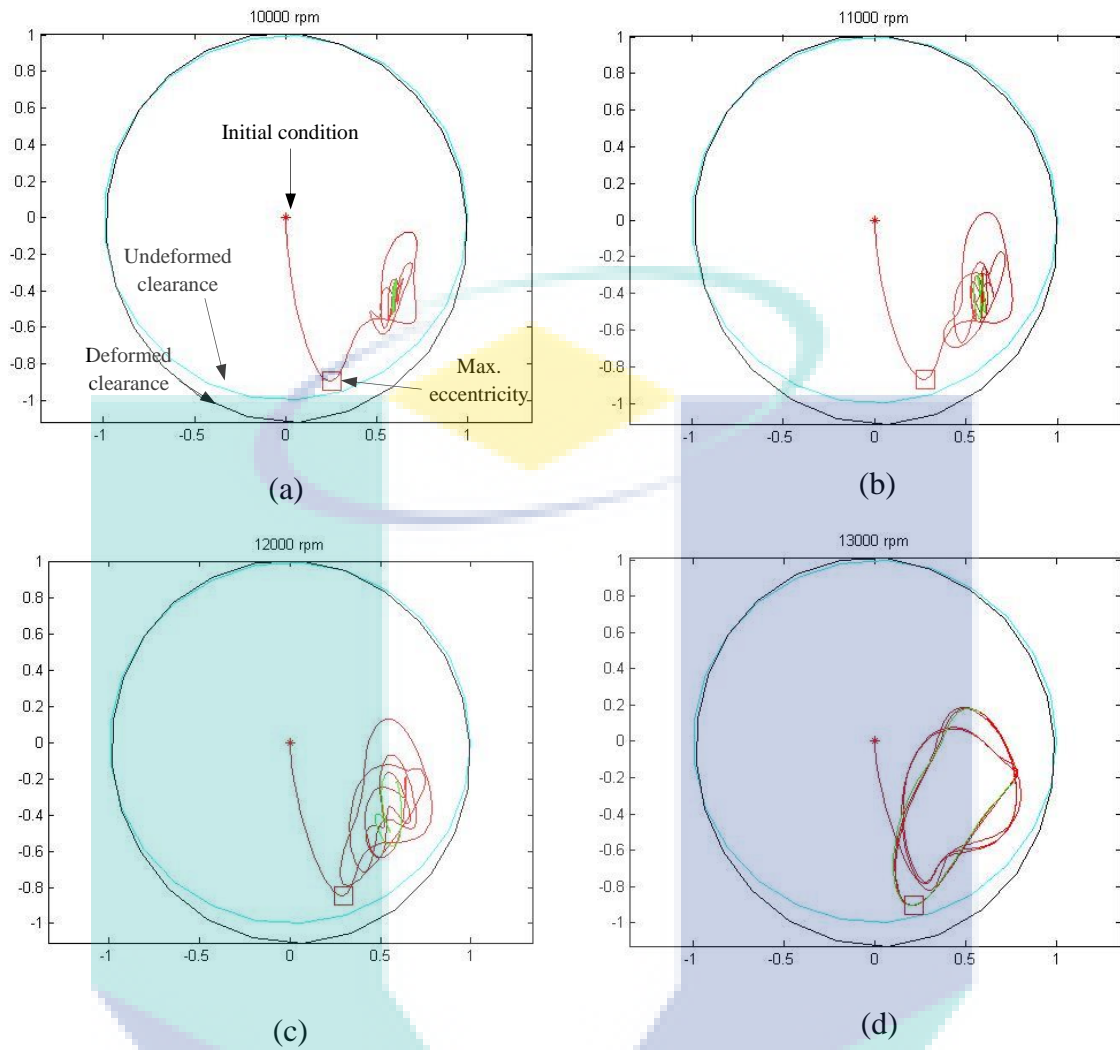
Figure 4.3:   Transient journal trajectory over 12 revs with m_ru = 5 g.mm at (a) 10,000 rpm; (b) 11,000 rpm; (c) 12,000 rpm; (d)13,000 rpm.
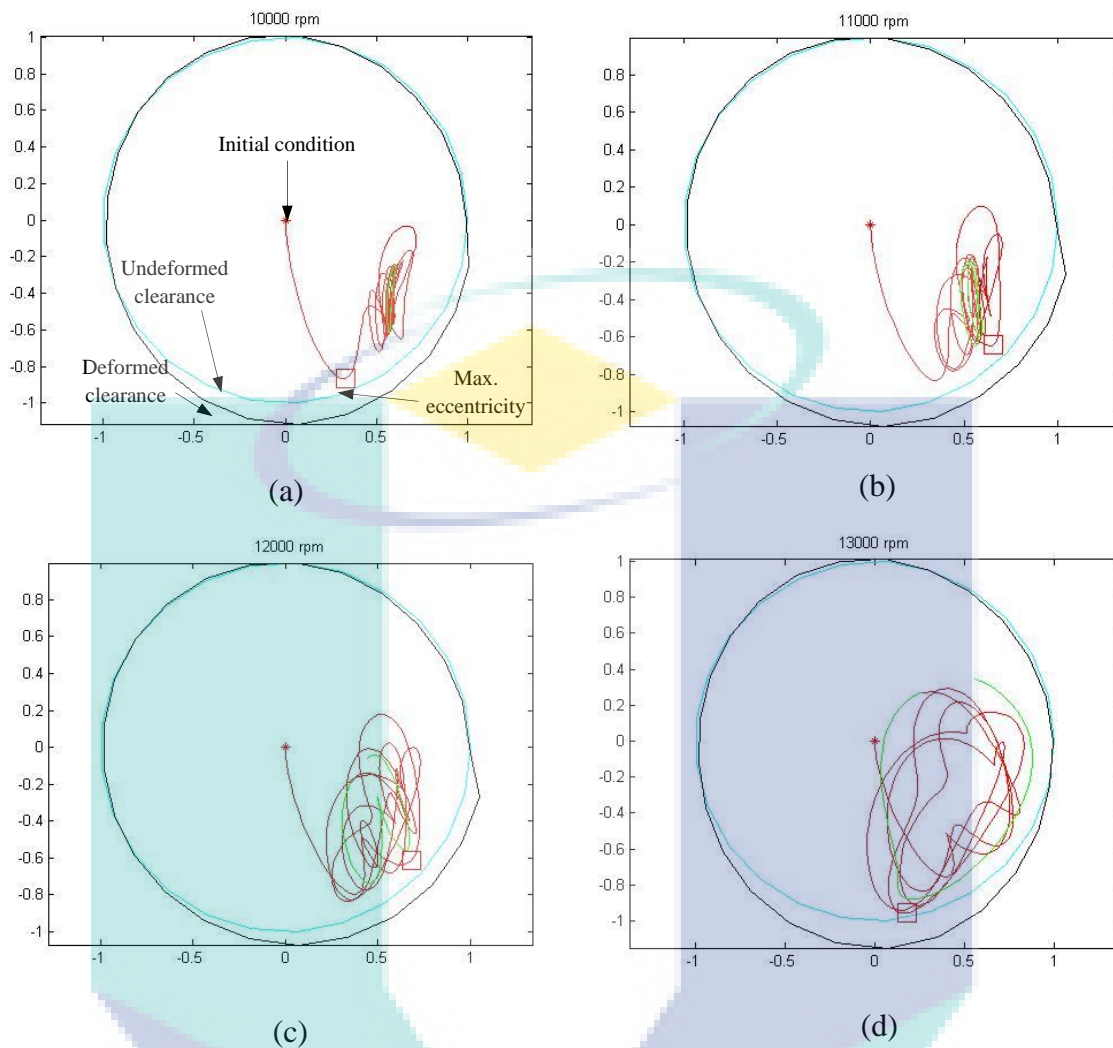
Figure 4.4: Transient journal trajectory over 12 revs with $m_r u$ = 10 g.mm at (a) 10,000 rpm; (b) 11,000 rpm; (c) 12,000 rpm; (d)13,000 rpm.

The coding had been run four speeds in the range 10,000 to 13,000 rpm with different value of $m_r u$ in FFSMM solution. From the Figure above, it showed that the trajectory converges to a stable static equilibrium position in 10,000 to 12,000 rpm. However, at 13,000 rpm the static equilibrium becomes unstable even though different value of $m_r u$. It is because this speed is quite close to instability speed range which is 13,587 rpm. This has been observed experimentally in[53]. In the Figure above also show the clearance deformation (due to the foil deflection) at the instant of maximum shaft eccentricity. The last point of the trajectory is the last position of the centre of the shaft after rotate at the certain rpm speed.

4.3   Verification and Validation of Rotor-Bearing Model against Published Results

Ruscitto et al. [54] published experimental data for the standard first-generation bearing used in this paper. This paper had been used until now for researched to validate their bearing models. Ruscitto et al measured the altitude angle under steady-state static loading condition over a certain range of static loads. The test was obtained utilizing the oscilloscope trace of the film thickness profile. Angular orientation of the oscilloscope trace is the bearing was made by referencing the discontinuity in the trace of the gap in the smooth foil which was located 180º from the point where the load was being applied. The altitude angle is defined as the angle between the load line and the line between the bearing and journal centres. The altitude angle was scaled as the angle between the lead line and the midpoint of the region where the minimum film thickness occurs in paper [54]. Table 4.1 below showed the Ruscitto et al's data.

Table 4.1:   Experimental data in Ruscitto et at's paper

Speed (rpm)	Bearing Load (N)	Altitude Angle (º)
30,000	4.4	25
	41.1	20
	63.4	18
	90.1	15
	116.8	13
	142.3	12
45,000	18.9	25
	63.4	22
	98.3	18
	135.4	15
	163.0	14
55,000	18.9	28
	63.4	25
	107.0	22
	142.3	17
	169.0	15

Source: Ruscitto et al.

To compare and validate our FFSMM to Ruscitto et al's data, a new MATLAB® coding had been made to generate the altitude angle. The locus of static equilibrium journal position had been calculated in the coding. The speed of the locus is followed the

40

Ruscitto et al's data which are at 30,000, 45,000 and 55,000 rpm. Figure 4.5 showed the locus of journal static equilibrium positions the range 10N to 210N in non-dimension while Figure 4.6 in dimension for 30,000 rpm.
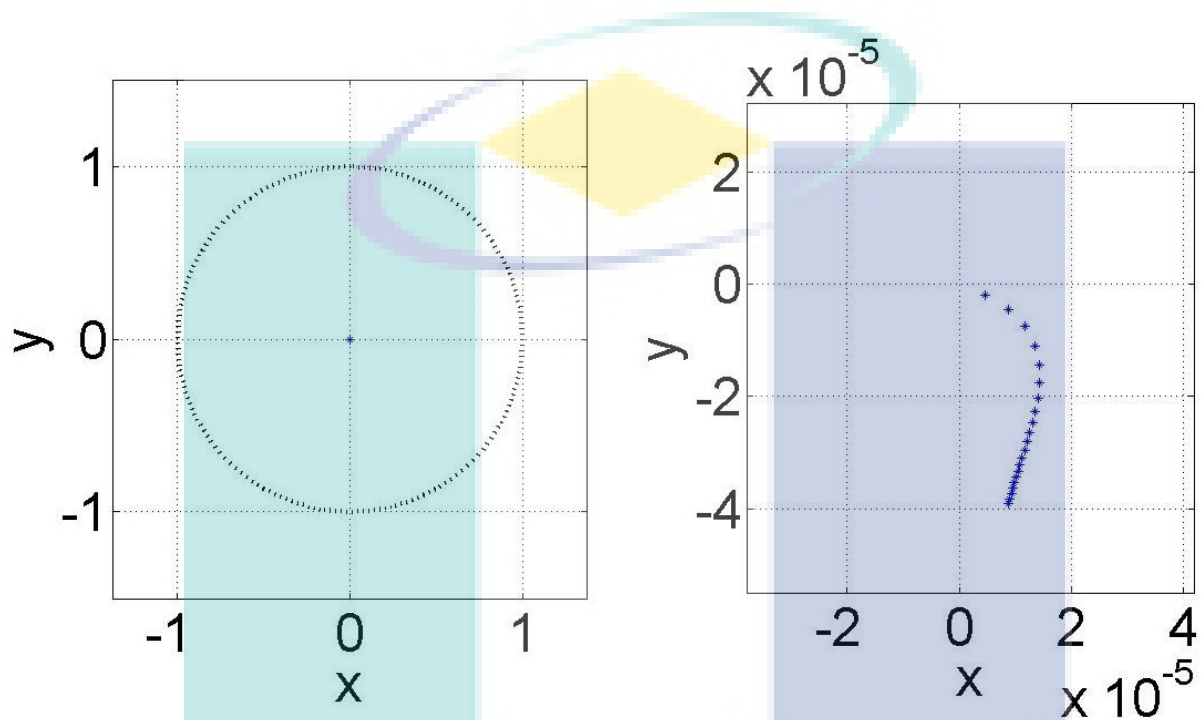
Figure 4.5: Predicted locus of journal static equilibrium positions at 30,000 rpm for static loads in the range 10N to 210N in dimensionless figure (a) before zoom (b) after zoom
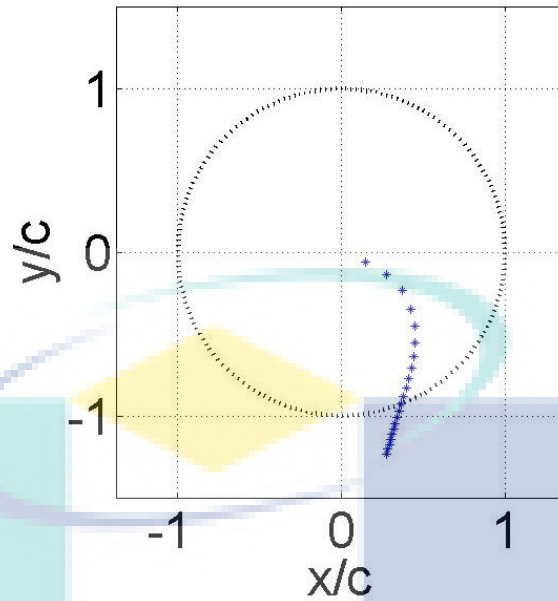
Figure 4.6:   Predicted locus of journal static equilibrium positions at 30,000 rpm for static loads in the range 10N to 210N in non-dimensionless figure
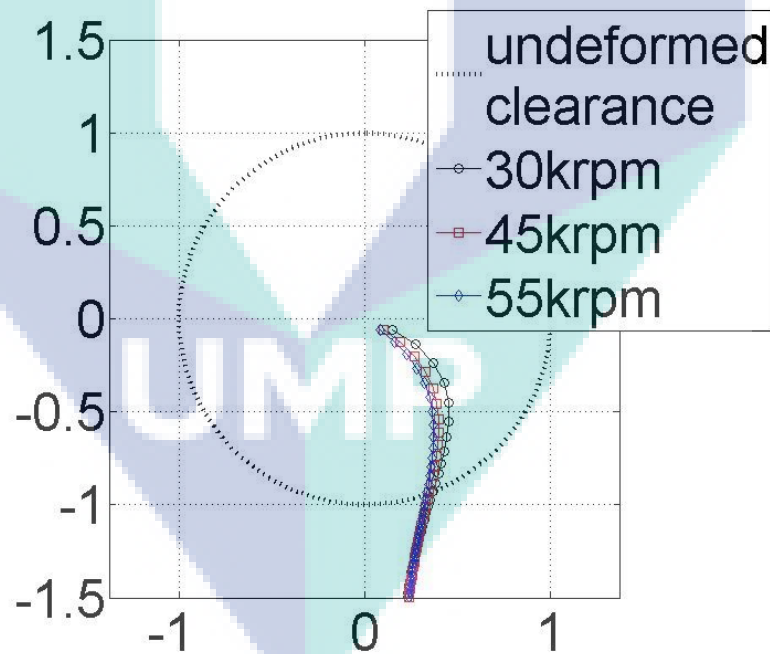
Figure 4.7:   Predicted locus of journal static equilibrium positions at 30,000 rpm, 45,000 rpm and 55,000 rpm for static loads in the range 10N to 210N in non-dimensionless figure

From the Figure above, an altitude angle can be calculate manually. The altitude angle that we get from the locus can be compared with Ruscitto et al's data. Figure 4.8 below showed the results of the comparisons.
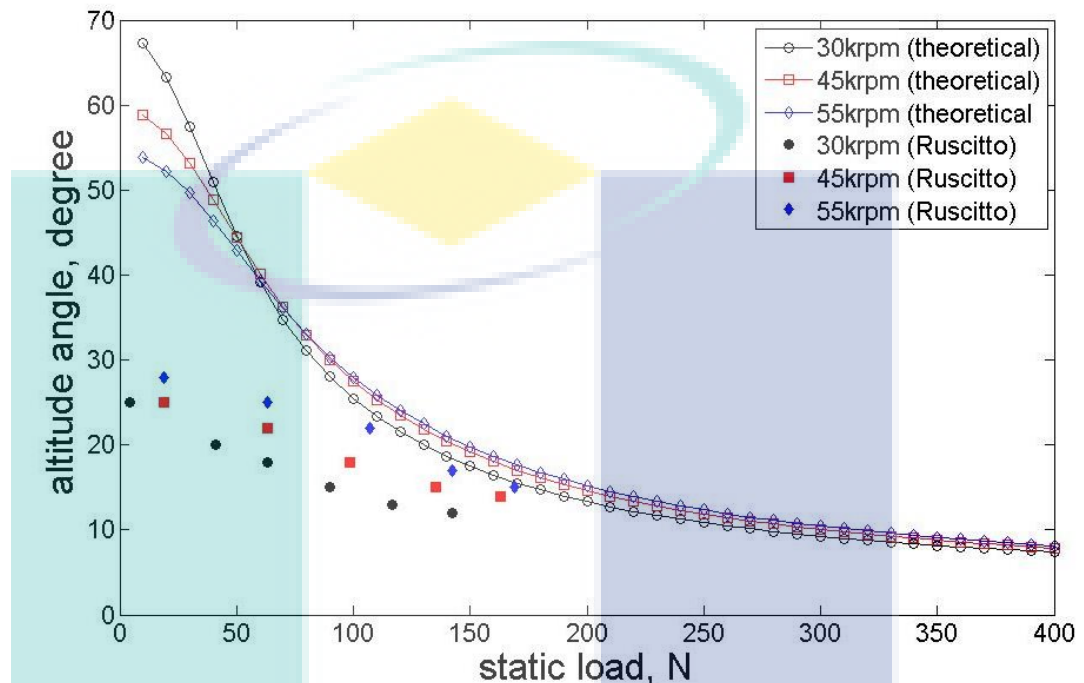
Figure 4.8:   Comparison between the FFSMM solution for altitude angle with
Ruscitto et al's altitude angle

Figure 4.8 shows that the results only a slight difference between the theoretical (FFSMM) and Ruscitto. The theoretical graph is accepted and can be used because as we can see that the shape of the graph is almost same with the Ruscitto. The difference between FFSMM and Ruscitto is the value of static load. FFSMM calculated from 0 N to 400N while Ruscitto only focused on smaller value of static load, 4.4N to 170N. We can predict that when the Ruscitto's static load is increase until 400N, the altitude angle will be same. This is because we can see that at the end of Ruscitto's data, the point is meet at the same point as the theoretical data. We can conclude that our graph can be used in predicted the high load, N while Ruscitto et al's graph is more focus on the smaller scale of load, N. From this comparison too, we can conclude that our method FFSMM is successfully calculated and integrated.

CHAPTER 5

CONCLUSION AND RECOMMENDATIONS

5.1 Introduction

The purpose of this chapter is to provide a review of this study's conclusion and recommendations. This chapter will described about the conclusion of this project, the future work and recommendation in continuing and improvement for this study.

5.2 Conclusion

This study has shown that the dynamics of the full foil structure of a first generation foil-air bearing (FAB) can be represented by a reduced modal model. In this study five modal models had been used. Full foil structure modal model (FFSMM) was successfully integrated. There is no effect of curvature for modelling the bump foil structure in the simultaneous solution. The FFSMM results were proven to be sound by comparison against those obtained experimental and theoretical results published in the literature for the static equilibrium condition. Besides that, the for this researched is identical with linear form of bearing. It showed that there is no effect of curvature for modelling the bump foil structure in the simultaneous solution. This solution can be used in high static load, N. This solution also can be used for the inclusion of more complex structures (Generation II, III designs) which until now was restricted to a simple spring damper models. The model can be easily adapted to include Coulomb friction forces, rather than equivalent viscous damping.

5.3 Recommendations

For this study, the inertia of the top foil was being ignored since the top foil of bearing was not being focussed in this study. For recommendation and improvement, others researched can include the top foil for the future study and compare the results.

Besides that, this study is focussed on 2D finite element modal analysis. The result for 2D finite element modal analysis is successfully proved in this paper. For next improvement, 3D finite element modal analysis can be developed and compare the final results to 2D modal analysis. Furthermore, this paper it discussed for the first generation of bearing (Generation I). So as recommendations, others researched can study on other bearings, Generation II and Generation III.
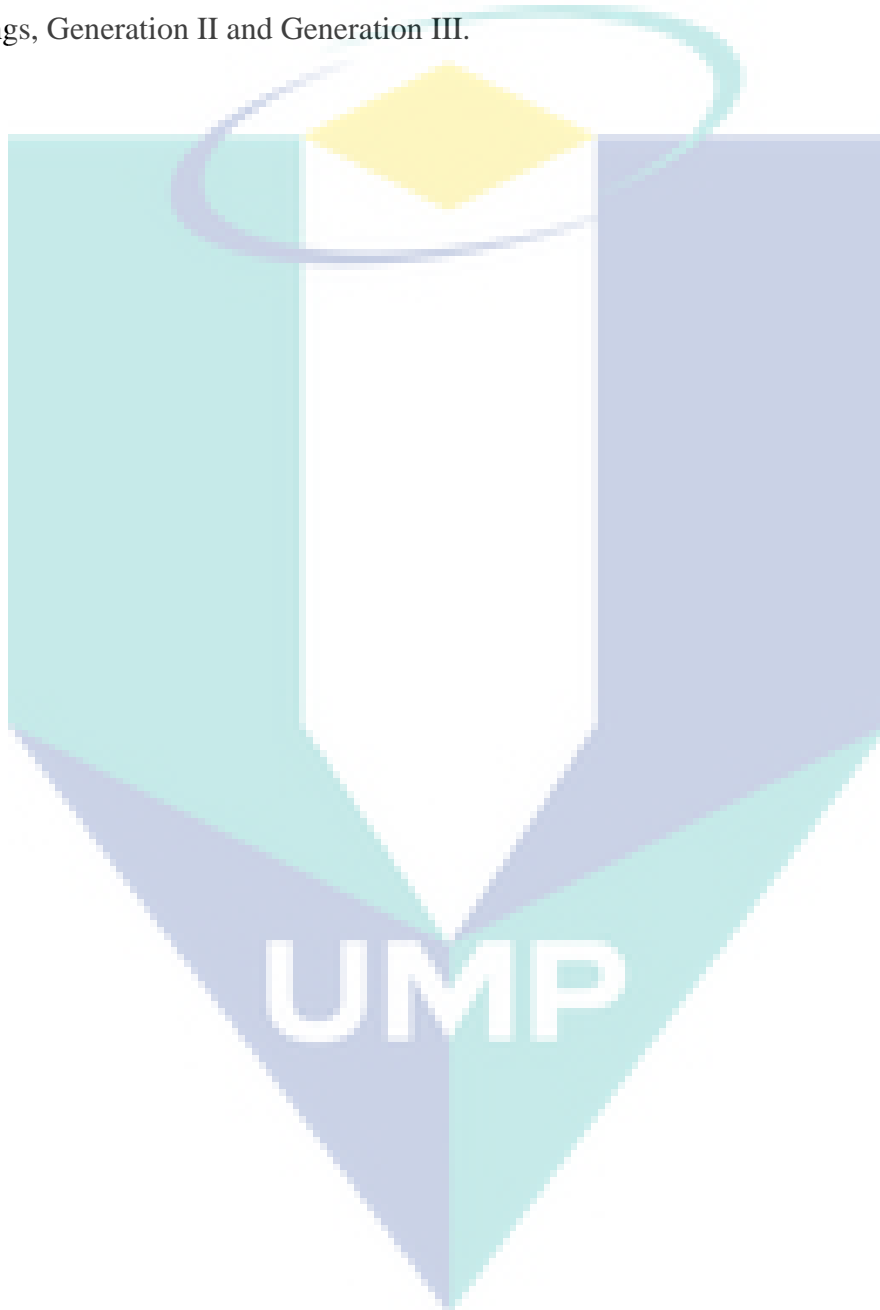
REFERENCES
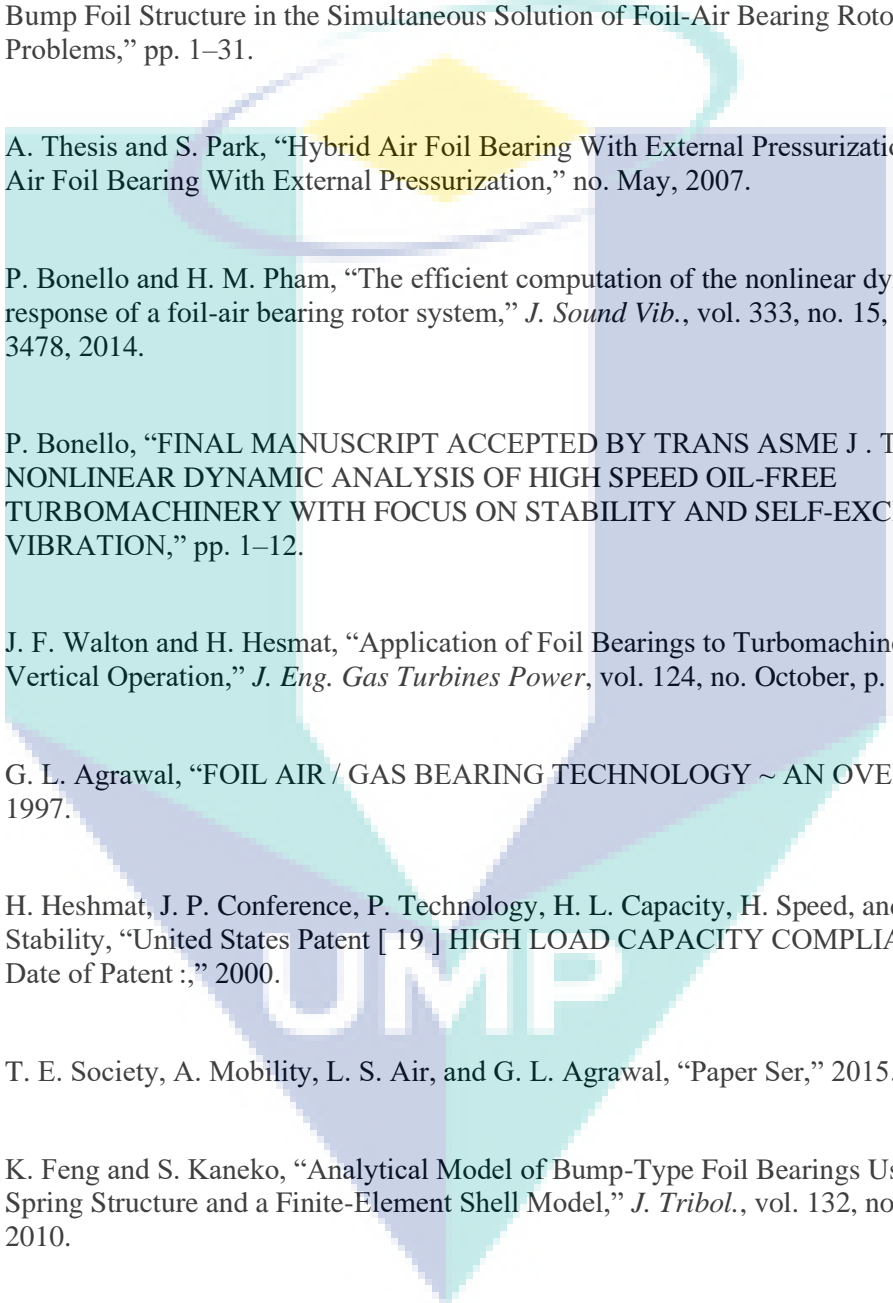
[1] C. Dellacorte, "A New Foil Air Bearing Test Rig for Use to 700°C and 70,000 rpm," *Tribol. Trans.*, vol. 41, no. 3, pp. 335–340, 1998.

[2] M. F. Bin Hassan and P. Bonello, "A New Modal-Based Approach for Modelling the Bump Foil Structure in the Simultaneous Solution of Foil-Air Bearing Rotor Dynamic Problems," pp. 1–31.

[3] A. Thesis and S. Park, "Hybrid Air Foil Bearing With External Pressurization Hybrid Air Foil Bearing With External Pressurization," no. May, 2007.

[4] P. Bonello and H. M. Pham, "The efficient computation of the nonlinear dynamic response of a foil-air bearing rotor system," *J. Sound Vib.*, vol. 333, no. 15, pp. 3459–3478, 2014.

[5] P. Bonello, "FINAL MANUSCRIPT ACCEPTED BY TRANS ASME J . TRIB . NONLINEAR DYNAMIC ANALYSIS OF HIGH SPEED OIL-FREE TURBOMACHINERY WITH FOCUS ON STABILITY AND SELF-EXCITED VIBRATION," pp. 1–12.

[6] J. F. Walton and H. Hesmat, "Application of Foil Bearings to Turbomachinery Including Vertical Operation," *J. Eng. Gas Turbines Power*, vol. 124, no. October, p. 1032, 2002.

[7] G. L. Agrawal, "FOIL AIR / GAS BEARING TECHNOLOGY ~ AN OVERVIEW," 1997.

[8] H. Heshmat, J. P. Conference, P. Technology, H. L. Capacity, H. Speed, and W. Stability, "United States Patent [19] HIGH LOAD CAPACITY COMPLIANT FOIL Date of Patent :," 2000.

[9] T. E. Society, A. Mobility, L. S. Air, and G. L. Agrawal, "Paper Ser," 2015.

[10] K. Feng and S. Kaneko, "Analytical Model of Bump-Type Foil Bearings Using a Link-Spring Structure and a Finite-Element Shell Model," *J. Tribol.*, vol. 132, no. 2, p. 21706, 2010.

[11] J. B. Oil-free, C. Dellacorte, and M. J. Valco, "Load Capacity Estimation of Foil Air « Kr '," no. October, 2000.

[12] N. K. Arakere and H. D. Nelson, "An Analysis of Gas-Lubricated Foil-Journal Bearings," *Tribol. Trans.*, vol. 35, no. 1, pp. 1–10, 1992.

[13]   H. Yu, C. Shuangtao, C. Rugang, Z. Qiaoyu, and Z. Hongli, "Tribology International Numerical study on foil journal bearings with protuberant foil structure," *Tribiology Int.*, vol. 44, no. 9, pp. 1061–1070, 2011.

[14]   M. Branagan, D. Griffin, C. Goyne, and A. Untaroiu, "Compliant Gas Foil Bearings and Analysis Tools," *J. Eng. Gas Turbines Power*, vol. 138, no. 5, p. 54001, 2015.

[15]   C. Dellacorte *et al.*, "Design , Fabrication , and Performance of Open Source Generation I and II Compliant Hydrodynamic Gas Foil Bearings Design , Fabrication , and Performance of Open Source Generation I and II Compliant Hydrodynamic," vol. 2004, no. December 2015, 2008.

[16]   T. H. Kim and L. S. Andrés, "Analysis of advanced gas foil bearings with piecewise linear elastic supports," *Tribol. Int.*, vol. 40, no. 8, pp. 1239–1245, 2007.

[17]   P. Taylor *et al.*, "Thrust Bump Air Foil Bearings with Variable Axial Load : Theoretical Predictions and Experiments Thrust Bump Air Foil Bearings with Variable Axial Load :," no. May 2013, pp. 37–41, 2011.

[18]   M. Carpino and G. Talmage, "A Fully Coupled Finite Element Formulation for Elastically Supported Foil Journal Bearings," *Tribol. Trans.*, vol. 46, no. 4, pp. 560–565, 2003.

[19]   C. Heshmat, D. Xu, and H. Heshmat, "Analysis of Gas Lubricated Foil Thrust Bearings using Coupled Finite Element and Finite Difference Methods," *ASME J. Tribol.*, vol. 122, no. January, pp. 199–204, 2000.

[20]   H. Heshmat, "Advancements in the performance of aerodynamic foil journal bearings: high speed and load capability.," *ASME J. Tribol.*, vol. 116, no. April, pp. 287–294, 1994.

[21]   M. Kumar and D. Kim, "Static performance of hydrostatic air bump foil bearing," *Tribol. Int.*, vol. 43, no. 4, pp. 752–758, 2010.

[22]   K. Harvey and P. Bonello, "Tribology International Improved identification of squeeze-film damper models for aeroengine vibration analysis," *Tribiology Int.*, vol. 43, no. 9, pp. 1639–1649, 2010.

[23]   J. S. Larsen and I. F. Santos, "Efficient solution of the non-linear Reynolds equation for compressible fluid using the finite element method."

[24]   K. Feng and S. Kaneko, "Thermohydrodynamic Study of Multiwound Foil Bearing Using Lobatto Point Quadrature," *J. Tribol.*, vol. 131, no. 2, p. 21702, 2009.

[25]   L. San Andrés and T. H. Kim, "Analysis of gas foil bearings integrating FE top foil models," *Tribol. Int.*, vol. 42, no. 1, pp. 111–120, 2009.

[26]   M. Arghir, S. Le Lez, and J. Frene, "Finite-volume solution of the compressible Reynolds equation: linear and non-linear analysis of gas bearings," *Proc. Inst. Mech. Eng. Part J J. Eng. Tribol.*, vol. 220, no. 7, pp. 617–627, 2006.

[27]   P. Taylor, M. J. Braun, F. K. Choy, M. Dzodzo, and J. Hsu, "Steady-State and Transient Dynamic Simulation of a Continuous Foil Bearing Steady-State and Transient Dynamic Simulation of a Continuous Foil Bearing @," no. March 2013, pp. 37–41, 2008.

[28]   K. H. Groves, P. Bonello, and P. M. Hai, "Proceedings of the Institution of Mechanical Engineers , Part C : Journal of Mechanical Engineering Science," 2012.

[29]   C.-C. Wang and C.-K. Chen, "Bifurcation Analysis of Self-Acting Gas Journal Bearings," *J. Tribol.*, vol. 123, no. 4, p. 755, 2001.

[30]   J. Schiffmann, "Foil Bearing Design Guidelines for Improved Stability," vol. 135, no. January, pp. 1–11, 2013.

[31]   A. M. Gad and S. Kaneko, "A New Structural Stiffness Model for Bump-Type Foil Bearings: Application to Generation II Gas Lubricated Foil Thrust Bearing," *J. Tribol.*, vol. 136, no. October, p. 41701, 2014.

[32]   M. F. Bin Hassan and P. Bonello, "A New Approach for Modelling the Foil Structure in the Simultaneous Solution of Foil-Air Bearing Rotor Dynamic Problems."

[33]   P. Bonello, "GT2013-94389 EFFICIENT TECHNIQUES FOR THE COMPUTATION OF THE NONLINEAR," pp. 1–9, 2013.

[34]   G. Grau, I. Iordanoff, B. B. Said, and Y. Berthier, "An original definition of the profile of compliant foil journal gas bearings: Static and dynamic analysis," *Tribol. Trans.*, vol. 47, no. 2, pp. 248–256, 2004.

[35]   J. S. Larsen, A. C. Varela, and I. F. Santos, "Tribology International Numerical and experimental investigation of bump foil mechanical behaviour," *Tribiology Int.*, vol. 74, pp. 46–56, 2014.

[36]   J. S. Larsen, A. J. T. Hansen, and I. F. Santos, "M echanics I ndustry Experimental and theoretical analysis of a rigid rotor supported by air foil bearings," vol. 106, 2015.

[37]   D. Rubio and L. San Andres, "Structural Stiffness, Dry Friction Coefficient, and Equivalent Viscous Damping in a Bump-Type Foil Gas Bearing," *J. Eng. Gas Turbines Power*, vol. 129, no. April, p. 494, 2007.

[38]   K. Rani and R. S. Gorayan, "(Experimental Investigation)," vol. 60, no. 12, pp. 579–583, 2013.

[39]   K. Feng and S. Kaneko, "Parametric Studies on Static Performance and Nonlinear Instability of Bump-Type Foil Bearings *," vol. 4, no. 6, pp. 1249–1257, 2010.

[40]   C. R. Ku, "Theoretical Model Including Strip," no. April, 1992.

[41]   D. K. Ã and S. Park, "Tribology International Hydrostatic air foil bearings : Analytical and experimental investigation," vol. 42, pp. 413–425, 2009.

[42]   P. Taylor, C. Dellacorte, and M. J. Valco, "Load Capacity Estimation of Foil Air Journal Bearings for Oil-Free Turbomachinery Applications Load Capacity Estimation of Foil Air Journal Bearings for Oil-Free Turbomachinery ~ ~ ~ l i c a t i o n s @," no. March 2013, pp. 37–41, 2008.

[43]   J. Song and D. Kim, "Compression Springs : Analyses and Experiments," vol. 129, no. July, 2007.

[44]   D. Lee, Y. Kim, and K. Kim, "Tribology International The effect of Coulomb friction on the static performance of foil journal bearings," *Tribiology Int.*, vol. 43, no. 5–6, pp. 1065–1072, 2010.

[45]   Y. L. Ã, D. Park, C. Kim, and S. Kim, "Operating characteristics of the bump foil journal bearings with top foil bending phenomenon and correlation among bump foils," vol. 41, pp. 221–233, 2008.

[46]   J. P. Peng and M. Carpino, "Coulomb Friction Damping Effects in Elastically Supported Gas Foil Bearings," *Tribol. Trans.*, vol. 37, no. 1, pp. 91–98, 1994.

[47]   S. Le Lez, M. Arghir, and J. Frene, "A New Foil Bearing Dynamic Structural Model," *ASME/STLE 2007 Int. Jt. Tribol. Conf. Parts A B*, vol. 129, no. October 2007, pp. 993–995, 2007.

[48]   S. Le Lez, M. Arghir, and J. Frene, "A Dynamic Model for Dissipative Structures used in Bump-Type Foil Bearings," *Tribol. Trans.*, vol. 52, no. 1, pp. 36–46, 2008.

[49]   S. Le Lez, "Nonlinear Numerical Prediction of Gas Foil Bearing Stability and," vol. 131, no. January, 2009.

[50]   D.-H. Lee, Y.-C. Kim, and K.-W. Kim, "The Dynamic Performance Analysis of Foil Journal Bearings Considering Coulomb Friction: Rotating Unbalance Response," *Tribol. Trans.*, vol. 52, no. 772815469, pp. 146–156, 2009.

[51]   P. Bonello, "GT2014-25176," pp. 1–10, 2014.

[52]   J. S. Larsen, I. F. Santos, and S. von Osmanski, "Stability of rigid rotors supported by air foil bearings: Comparison of two fundamental approaches," *J. Sound Vib.*, vol. 381, pp. 179–191, 2016.

[53]   J. S. Larsen and I. F. Santos, "On the nonlinear steady-state response of rigid rotors supported by air foil bearings — Theory and experiments," *J. Sound Vib.*, vol. 346, pp. 284–297, 2015.

[54]   S. G. D. Ruscitto, J. Mc Corm_ck, "COMPLIANT PERFORMANCE AIR LUBRICATED ENGINE BEARING FOR AN AUTOMOTIVE," *J. Bear. Perform.*, 1978.